5-2010

Thermo-Mechanical Reliability of Micro-Interconnects in Three-Dimensional Integrated Circuits: Modeling and Simulation

Omar Rodriguez
Utah State University

THERMO-MECHANICAL RELIABILITY OF MICRO-INTERCONNECTS IN THREE-DIMENSIONAL INTEGRATED CIRCUITS: MODELING AND SIMULATION

by

Omar Rodriguez

A thesis submitted in partial fulfillment
of the requirements for the degree

of

MASTER OF SCIENCE

in

Mechanical Engineering

Approved:

_____	_____
Dr. Leila Ladani Major Professor	Dr. Thomas Fronk Committee Member
_____	_____
Dr. Byard Wood Committee Member	Dr. Byron Burnham Dean of Graduate Studies

UTAH STATE UNIVERSITY
Logan, Utah

2010

ABSTRACT

Thermo-Mechanical Reliability of Micro-Interconnects in Three-Dimensional Integrated Circuits: Modeling and Simulation

by

Omar Rodriguez, Master of Science

Utah State University, 2010

Major Professor: Dr. Leila Ladani
Department: Mechanical Engineering

Three-dimensional integrated circuits (3D ICs) have been designed with the purpose of achieving higher communication speed by reducing the interconnect length between integrated circuits, and integrating heterogeneous functions into one single package, among other advantages. As a growing, new technology, researchers are still studying the different parameters that impact the overall lifetime of such packages in order to ensure the customer receives reliable end products. This study focused on the effect of four design parameters on the lifetime of the interconnects and, in particular, solder balls and through-silicon vias (TSVs). These parameters included TSV pitch, TSV diameter, underfill stiffness and underfill thickness. A three-dimensional finite element model of a 3D IC package was built in ANSYS to analyze the effect of these parameters under thermo-mechanical cyclic loading. The stresses and damage in the interconnects of the IC were evaluated using Coffin-Manson and the energy partitioning fatigue damage models. A three-level Taguchi design of experiment method was utilized to evaluate the effect of each parameter. Minitab software was used to

assess the main effects of the selected design parameters. Locations of maximum stresses and possible damage initiation were discussed, and recommendations were made to the manufacturer for package optimization.

Due to the very small scale of the interconnects, conducting mechanical tests and measuring strains in small microscopic scale material is very complicated and challenging; therefore, it is very difficult to validate finite element and analytical analysis of stress and strain in microelectronic devices. At the next step of this work, a new device and method were proposed to facilitate testing and strain measurements of material at microscopic scale.

This new micro-electromechanical system (MEMS) consisted of two piezoelectric members that were constrained by a rigid frame and that sandwiched the test material. These two piezoelectric members act as load cell and strain measurement sensors. As the voltage is applied to the first member, it induces a force to the specimen and deforms it, which in turn deforms the second piezoelectric member. The second piezoelectric member induces an output voltage that is proportional to its deformation. Therefore, the strain and stresses in the test material can be determined by knowing the mechanical characteristics of the piezoelectric members. Advantages of the proposed system include ease of use, particularly at microscopic scale, adaptability to measure the strain of different materials, and flexibility to measure the modulus of elasticity for an unknown material. An analytical analysis of the device and method was presented, and the finite element simulation of the device was accomplished. The results were compared and discussed. An inelastic specimen was also analyzed and sensitivity of the device to detecting nonlinear behavior was evaluated. A characteristic curve was developed for the specific geometry and piezoelectric material.

(75 pages)

ACKNOWLEDGMENTS

I would like to thank Dr. Leila Ladani and the Micron Research Center for giving me the opportunity to work with them in this project. It helped me to grow personally and professionally.

I want to thank my family, especially my mom and dad for always being there for me spiritually and never allowing me to give up. Also, I want to thank my unconditional friends. They were in part the reason that kept me sane through all these years. I dedicate this work to my professors and staff in the MAE department and all through Utah State University who helped this in being a wonderful (and painful at times) experience.

Additionally, I want to thank the government of the Dominican Republic for sponsoring my education at Utah State University for the past five years.

Omar Rodríguez

CONTENTS

LIST OF TABLES

LIST OF FIGURES

CHAPTER 1

INTRODUCTION AND OBJECTIVES

1.1. Introduction

The electronic industry is moving towards the miniaturization of all the electronics components in order to achieve higher speeds and more functionality. Three-dimensional integrated circuits (3D ICs) are a relatively new packaging technology consisting of stacking different integrated circuits vertically to achieve higher speed, better form factor, increased functionality, and heterogeneous functions in one package. 3D ICs are the future in integration technology with the promise of faster communication between electronic devices. Current 2D technologies have reached a point at which it has become economically unfeasible to produce integrated circuits that can exceed the current technology trend in terms of processing time.

As the size of the package is reduced, interconnect size is also reduced to nano and microscopic scale. Several of these packages consist of thousands of interconnects. The probability of failure of a package increases as the number of interconnects increases in high-density packages. Furthermore, many of these packages are used in applications in which they experience a variety of loads, such as thermo-mechanical, mechanical cyclic loading, and vibration.

Mechanical stresses are induced in interconnects due to coefficient of thermal expansion mismatch between the different layers of the package. Therefore, it is important at the design stage to know or to be able to estimate the reliability of these interconnects. Chapter 2 deals with this topic. A parametric study of design factors, such as interconnects size, pitch, die thickness and modulus of elasticity of underfill material, is conducted using finite element modeling.

An experiment is designed in which these parameters are varied according to a Taguchi design. Three levels are selected to obtain any nonlinear relationship between the response parameter and factors. Finite element analysis is used to determine the critical location of failure for the interconnects and critical level of each parameter. In addition, two reliability models, Coffin-Manson and energy-partitioning method, are used to determine the number of cycles to failure for the copper and solder interconnects, respectively, and to determine the variations of cycles to failure based on design parameters. The thermal load consists of a 125°C hot dwell for 15min, a steady decrease at a rate of 10°C/min, followed by a -55°C cold dwell for 10min, and steady increase at a rate of 6°C/min. For the finite element analysis, the solder ball is modeled as a viscoplastic material experiencing both time dependent and independent deformations. The steady state secondary creep strain rate is modeled with Garofalo's equation, which models the secondary creep strain rate as a function of the stress level that the copper is subjected to and the operating temperature; the time independent deformation is modeled using a power-law series.

In order to assess the life of the solder ball, the energy-partitioning method, a continuum damage model, is utilized. The lifetime of the solder ball is determined by superimposing the damage due to the elastic, plastic, and creep energy densities. A power-law series is used to approximate the number of cycles to failure based on each of the energy densities. The damage is then calculated as the inverse of the cycles to failure, and ultimately the total damage of the solder ball is obtained by adding the damage due to the elastic, plastic, and creep deformation.

The life of the through-silicon via (TSV) is determined by the Coffin-Manson damage model. This model is used to model lifecycle for cyclic fatigue due to plastic strain deformation and follows a power-law series.

Finite element analysis only provides an estimation of the reliability based on plastic strain, or plastic and creep work density observed. However, it is important to confirm the results of this model with experiments. Currently, experimental techniques for fatigue testing and strain measurements at the microscopic scale are very limited. To conduct fatigue testing, an experiment is proposed to develop a micro-electromechanical machine able to test specimens at nano and microscopic scales. Strain measurement has been the object of many studies, and has been accomplished through the utilization of different methods. These methods extend from x-ray diffraction, capacitive, photoelastic, or magnetoelastic strain gauges. Disadvantages of these methods include disability to measure large deformations, complicated equipment needed to measure strain, need to embed the measuring device on the material, and inability of measuring strain at the microscopic scale.

In Chapter 3 a new device and methodology that can be applied at the microscopic scale to measure strain on specimens is proposed. Its design consists of two piezoelectric members that sandwich the test material; one piezoelectric material acts as a load cell, the second acts as a strain sensor. Strain and stress are measured through an input and output voltage that is related to the strain and stress by means of piezoelectric material constants. Advantages of this system include ease of use particularly at microscopic scale, adaptability to measure the strain of different materials, and flexibility to measure the modulus of elasticity for unknown material. In addition, it can easily be used to test the material for fatigue. Analytical and finite element approaches are used to determine the feasibility of

technique and the strains calculated through the output voltage, analytically and with finite element, show good correlation. . Alternatively, testing materials to determine their modulus of elasticity can be achieved using the same principle of relating the input and output voltage relations. This capability can be later implemented in testing materials for cyclic loading, to determine how the modulus of elasticity is affected by cycling and in determining the S-N curve for various types of materials.

1.2. Significance and Objectives

This research is motivated by the need of overcoming the challenges new technologies face during their initial stages. At this point, a reliability analysis of three-dimensional ICs is necessary to understand the impact that the operational conditions have on the durability of these components. Without this understanding, the technology would be rendered unreliable, as the impact of the design parameters would not be understood and operational conditions could induce failure of the ICs at the early life stage.

To accomplish this reliability study, it becomes a necessity to measure the material's strain and stress at the microscopic level. It is well-known that materials exhibit different behavior at the macroscopic scale. At the microscopic scale, the continuum mechanics theory breaks down and cannot be utilized; therefore, different models have to be developed to understand the behavior of material at the microscopic level. Additionally, it becomes hard to perform accurate measurements at the microscopic level as complicated machinery is usually required to achieve the measurements, the measuring device is sometimes embedded on the material being tested, and complicated test configurations are required for some techniques, among other reasons. For this reason, a piezoelectric microstrain measurement device to overcome the difficulty of measurements at the microscopic level is proposed.

The main objectives of this study are:

- to assess durability of the interconnects of three-dimensional integrated circuits subjected to thermo-mechanical loading;
- to recommend different geometry that would optimize the overall lifetime of the integrated circuit;
- to design a device to facilitate measuring deformation and fatigue for microscopic specimens by means of piezoelectricity;
- to develop a characteristic plot for the specified geometry as a function of the modulus of elasticity of the specimen being tested.

CHAPTER 2

STRESS ANALYSIS OF MICRO-INTERCONNECTS IN THREE-DIMENSIONAL INTEGRATED CIRCUITS

2.1. Introduction and Literature Review

Electronic packaging is moving towards the miniaturization of all the electronics components in order to achieve higher speeds and more functionality. Three-dimensional integrated circuits (3D ICs) are a relatively new packaging technology consisting of stacking different integrated circuits vertically. Advantages include better form factor (size miniaturization to increase density and capacity/volume ratio), integration of heterogonous functions in a single package, e.g. processor, logic, and memory, utilization of short vertical interconnects instead of long 2D interconnects to increase electrical performance level, parallel processing, low power consumption [1,2], among other advantages. However, since this is a new technology, many different aspects have to be considered, specifically the effect of temperature in the integrated circuits interconnects to determine the life and reliability of the integrated circuit.

In order to achieve interconnections at the microscopic level, different technologies have been proposed, such as direct bonding, solid liquid inter-diffusion bonding, surface activated bonding, and direct chip attach (DCA); the latter being one of the oldest techniques used to connect the silicon layers to a substrate using small solder joints and underfill. The architecture considered in this study uses DCA bonding.

Adjacent layers of active dies are connected with through-silicon vias (TSVs), an interconnect technology well-known for being used by important electronic companies, such as IBM [3] and Intel [4]. The lifetime of TSVs is mainly affected by environmental temperature cycling or thermally-induced stresses at the operational temperature. Bloomfield

et al. [5] and Zhang et al. [6] investigated these stresses using two different approaches. They concluded that stresses developed in TSV may exceed the yield stress, and that stress depends on some design parameters, such as TSV pitch and TSV diameter.

As the silicon layers are stacked, the structure becomes more cubical, and a large amount of stiff material will surround the TSVs and other interconnects. Such high stiffness prevents large deformation in the package due to a thermo-mechanical mismatch between the different materials the IC is composed of. For this reason, the underfill material plays the role of reducing thermal coefficient mismatch, and consequently reduces the amount of deformation increasing the durability of the TSVs. Therefore, optimizing intermediate layers may be a key to enhancing reliability of interconnects.

For these reasons, it is understood that it is important to assess the lifetime of the TSV interconnects as the thermo-mechanical loading may induce early failure in the life of the 3D IC. The main design parameters that will impact durability of the TSVs have to be studied and understood. A study conducted by Khan et al. [7], from the Institute for Microelectronic (IME), showed that TSV life could be as low as 500 cycles under accelerated thermal cyclic loading. Hsieh and Yu [8] modeled TSVs in a 3D package and found that maximum stress occurs between the TSV and silicon layer due to the large coefficient of thermal expansion mismatch. Therefore, TSV failure may very well be the main concern for future electronic manufacturers.

This study presents a numerical experiment conducted at three levels to observe the effect of different design parameters such as TSV diameter, TSV pitch, die thickness, underfill thickness, and underfill properties on the thermo-mechanical durability of solder joints and TSV copper interconnects.

2.2. Package Geometry and Architecture

Before going in-depth about the architecture of the 3D IC, it is necessary to establish the physical difference between 2D and 3D integrated circuits. Figure 1 shows a comparison between these two types of ICs. On the left, several 2D integrated circuits are shown; each one of these ICs executes a function it is designed for, and transmits the appropriate information to another IC in order for it to process or store. On the right, a 3D IC is shown; the 2D ICs from the left are now stacked on top of each other and operate as one integrated circuit achieving different functions in one package. The required space is reduced with 3D ICs since no packaging per individual 2D IC is required.

The geometry of the integrated circuit package is shown on Fig. 2. Solder balls are used to connect the silicon layers on the middle, in one row. Each active layer of silicon is connected to the next one with TSVs interconnects. One important element in utilizing TSVs is its aspect ratio, i.e. ratio of the die thickness to the TSV diameter, which indicates how miniaturized the system is. For this study it was kept constant at 5:1.

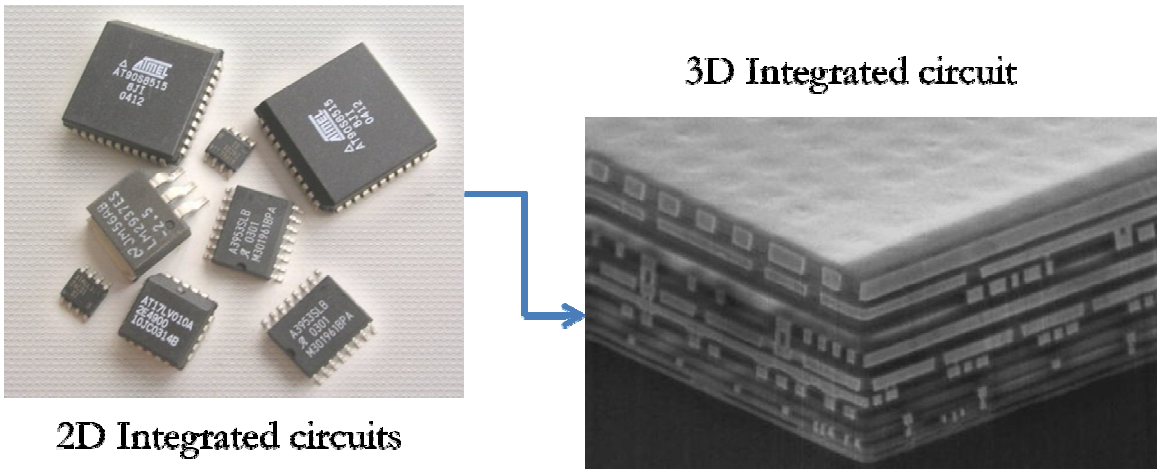

Figure 1. 2D IC vs. 3D IC comparison. [9,10]

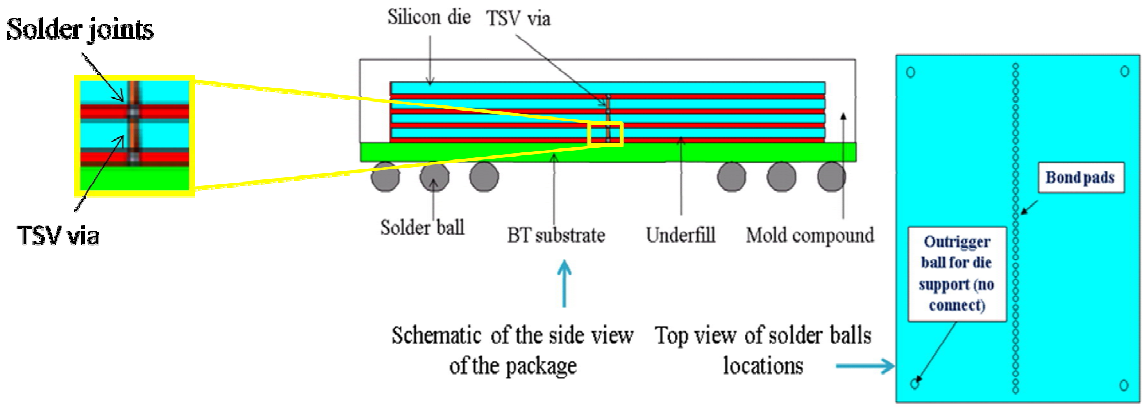

Figure 2. Schematic of the 3D IC package.

Table 1. Linear Mechanical and Thermo-Mechanical Properties of Materials

Material	Elastic Modulus E (MPa)	Coefficient of Thermal Expansion CTE (ppt)	Poisson's ratio ν
Molding compound	15.79E3	9	0.3
Silicon die	191E3	2.33	0.3
Copper	171E3	14.3	0.35
TB substrate	26E3	15	0.39
Underfill	3E3	30	0.3
Solder	4.37E4-22.3 T(K)	20.9	0.4

The size of each die is approximately 7 mm x 10 mm x 0.100 mm, and the package size is 8 mm x 11.5 mm x 1.0 mm. The 1.0-mm thickness includes 0.25 mm and 0.850 mm of substrate and molding compound thicknesses, respectively. A list of the mechanical and thermo-mechanical properties of all the materials is shown in Table 1.

2.3. Finite Element Analysis

A three-dimensional solid model of the package is built using ANSYS Parametric Design Language (ADPL). Due to symmetry of the package, only a quarter of the geometry was modeled. This is done in an effort to reduce the number of degrees of freedom and to

reduce computational time; only one strap of the package containing the TSV and solder joints is modeled.

Element SOLID185 is used in the solid model. This element is an 8-noded structural solid brick element with linear interpolation functions, which has the capability of modeling plasticity, stress stiffening, creep, large deflection, and large strain [11]. Displacement boundary conditions are applied such that symmetry faces are fixed in perpendicular directions, and the center of the package was fixed in all directions. The finite element model is shown in Fig. 3.

A thermal load is applied to the model; the thermal profile is shown on Fig. 4. The IC package is subjected to a high temperature of 125 °C for 15 minutes. The temperature is decreased at a rate of 10 °C/min for 18 minutes until reaching a low temperature of -55°C. The temperature is held constant at the low temperature for 10 minutes and then gradually increased at a rate of 6°C/min for 30 minutes until reaching a high temperature of 125°C again. The total time of the cycle is 73 minutes.

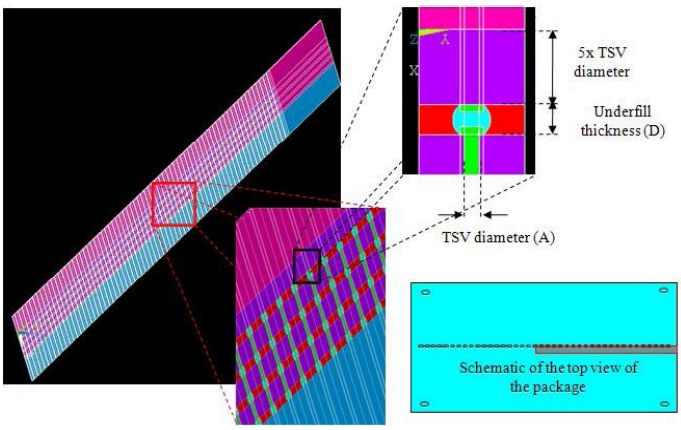

Figure 3. Finite element model containing TSVs and solder joints.

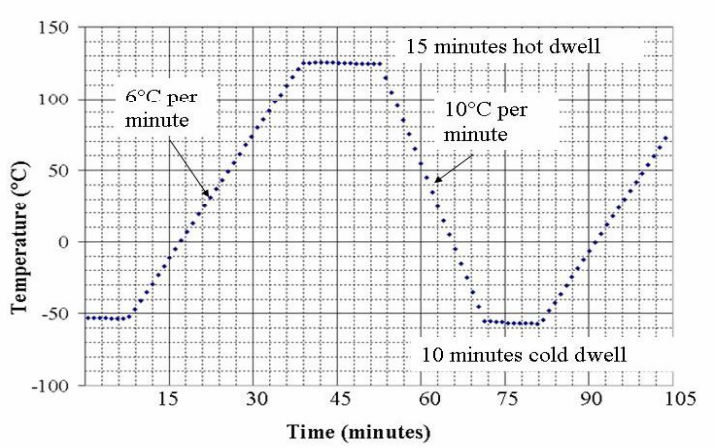

Figure 4. Thermal cycle applied to solid model.

To analyze the effect of each design parameter in the solid model, a Taguchi design of experiment (DOE) is used. This will be discussed in section 2.5. All specified runs are modeled in ANSYS, and the damage of the solder joints and the TSV copper interconnects is then assessed using energy-partitioning method and Coffin-Manson, respectively. The next section goes into detail of these two models and the constitutive properties of solder.

2.4. Damage Model and Nonlinear Constitutive Properties

A damage analysis is done for the copper TSV and the lead-free SAC (SnAgCu) solder joints. For the solder joints, the energy-partitioning model is used to determine the number of cycles to failure based on the amount of damage induced by the applied thermal load. Copper TSVs are modeled as bilinear isotropic hardened materials and the Coffin-Manson damage model is used to assess their durability.

The operational temperature for electronic packages is usually higher than half the homologous temperature for the copper TSV (the ratio of the actual temperature to the melting point in Kelvin) in the Ashby deformation map. For this reason solder will

experience both rate dependent and independent (creep and plasticity, respectively) inelastic deformation.

2.4.1. Energy-Partitioning Damage Model

The energy-partitioning (E-P) damage model is used to model cyclic fatigue [12]. This model predicts cyclic creep fatigue damage based on deviatoric elastic (U_e), plastic (W_p) and creep (W_c) energy densities. A power-law series is utilized to determine the damage due to each of the deformation mechanisms, respectively, i.e.

$$U_e = U_{e0} \cdot {N_{fe}}^{b}, \tag{1a}$$

$$W_p = W_{p0} \cdot {N_{fp}}^{c}, \tag{1b}$$

$$W_c = W_{c0} \cdot {N_{fc}}^{d}, \tag{1c}$$

where N_{fe}, N_{fp}, and N_{fc} are the number of cycles to failure for elastic, plastic and creep accordingly. U_{e0}, W_{p0}, and W_{c0} represent the intercept of the elastic, plastic and creep energy density plots versus cycles to failure, on a log-log plot, while the exponent b, c, and d are their corresponding slopes, respectively. These constants are material properties. Damage is defined as the reciprocal of the number of cycles as follows

$$D = \frac{1}{N_f}. \tag{2}$$

The total damage can be calculated by superimposing damage caused by elastic, plastic and creep deformation such that

$$D_{total} = D_e + D_p + D_c, \tag{3}$$

where D_e, D_p, and D_c are the elastic, plastic and creep damages, respectively. Usually damage caused by elastic deformation is negligible and is then eliminated from the equation. Damage caused by each type of deformation can be calculated by substituting Eqs. (1a), (1b) or (1c) into Eq. (2). Therefore, the total number of cycles to failure is then obtained as

$$\frac{1}{N_f} = \frac{1}{N_{fp}} + \frac{1}{N_{fc}}. \quad (4)$$

Damage model constants from Eqs. (1b) and (1c), i.e. W_{p0}, W_{c0}, c, and d are obtained from the literature for Pb-free solders [13]; the nominal values are 198, 123, -0.8, and -1.4, respectively. W_p and W_c are obtained from finite element analysis.

2.4.2. Coffin-Manson Model

To model the copper TSV interconnects, the Coffin-Manson damage model is used, which relates the number of cycles to failure to the inelastic strain amplitude during one cycle of loading by a power law series, such that

$$N_f = C(\Delta\varepsilon_i)^m. \quad (5)$$

The fatigue ductility coefficient C and fatigue exponent m are usually obtained experimentally for a specific material. These constants are size and process dependent. Therefore, constants are different for bulk and electroplated copper. In the case of TSV, constants for electroplated copper are obtained from literature and are 0.0121 and -2.455 for m and C, respectively [14].

2.4.3. Constitutive Properties

Due to the high temperatures the package exhibits, solder is modeled as a viscoplastic material, experiencing both rate-dependent and rate-independent inelastic deformation. A partitioned viscoplastic constitutive law is employed in the finite element analysis to facilitate the use of the energy-partitioning fatigue model,

$$\varepsilon = \varepsilon_e + \varepsilon_p + \varepsilon_{sc}, \quad (6)$$

where ε is total strain, ε_e is elastic strain, ε_p is rate-independent plastic strain and ε_{sc} is rate-dependent steady state (secondary) creep strain. The transient primary creep strains are

neglected because they cause negligible damage in thermal cycling. The rate-independent inelastic constitutive model is formulated as

$$\sigma = C_p \varepsilon_p^{n_p}, \tag{7}$$

where ε_p is equivalent plastic strain, and C_p and n_p are temperature-dependent material constants; they are summarized in Table 2. The steady-state secondary creep strain rate is described by Garofalo's equation [15] as

$$\frac{d\varepsilon_{sc}}{dt} = A\big(sinh(\alpha\sigma)\big)^{n_c} \cdot exp\left(-\frac{Q}{RT}\right), \tag{8}$$

where a is related to the stress level at which the power law dependence breaks down, Q is activation energy, A and n_c are model constants. Copper is considered to have bilinear isotropic behavior. Nonlinear constitutive properties of solder used in ANSYS are provided in Table 2.

2.5. Numerical Design of Experiment

During the design stage of the 3D ICs, it is important to understand the effect each design parameter has in the lifetime of the package. However, these design parameters are many, and result in a very large test matrix needed to determine the main effects. For this reason, only four of these parameters are chosen to be analyzed in this experiment. Those parameters consist of, TSV diameter, underfill thickness, underfill stiffness, and TSV pitch, each at three different levels. To maintain the aspect ratio constant at 5:1, the die thickness was also changed as the TSV diameter changed. Since this ratio is kept constant, these two variables are considered as one factor in the design of experiment (DOE).

Table 2. Nonlinear Constitutive Properties of Solder and Copper

SAC	**Plastic constants**		**Creep constants**			
	C_p	**n_p**	**A**	**α**	**n_c**	**Q (J/Mol)**
	121.6-0.4[T(ºC)]	0.29-0.00046[T (ºC)]	1.5E 3	0.19	4.0	7.13E4
TSV	**Yield stress (MPa)**		**Tangent modulus (MPa)**			
	172.3		517.1			

The four variables for this study and the levels selected for these variables are listed in Table 3. The test matrix for a conventional factorial experiment would require 4^3=64 runs. For this reason, a Taguchi orthogonal array is selected that will only require 9 different runs to be analyzed [16]. An L9 orthogonal array is selected and is shown in Table 4. Taguchi arrays allow the use of smaller test matrices, but carry a penalty in obtaining interaction effects for the simple fact that many of the interaction effects are confounded into main factor effects and cannot be separated.

The first column in Table 4 shows the run number and the DoE variables are placed in the subsequent columns: 1 refers to the low level of each variable; 2 represents the intermediate or nominal level; 3 refers to the high level.

Table 3. Parameters Varied in Three Levels

Parameter	1	2	3
TSV diameter, die thickness (A)	10, 50 μm	20, 100 μm	30, 150 μm
Underfill stiffness (B)	3GPa	6GPa	9GPa
TSV pitch (C)	70μm	95μm	120μm
Underfill thickness (D)	20μm	40μm	50μm

Table 4. Taguchi L9 Orthogonal Array

Run	A	B	C	D
1	1	1	1	1
2	1	2	2	2
3	1	3	3	3
4	2	1	2	3
5	2	2	3	1
6	2	3	1	2
7	3	1	3	2
8	3	2	1	3
9	3	3	2	1

2.6. Numerical Results and Conclusions

Data from the finite element solutions is analyzed after each run is completed. Data such as plastic strain energy, creep strain energy, elastic strain, as well as stresses is allocated in preset data tables. Data is arithmetically manipulated to compute the EP method lifetime for the solder balls, and the Coffin-Manson model lifetime for the copper TSVs; the manipulated data with the computed lifetime is stored in two element tables (ETABLEs), one for the solder ball, and one for the copper TSVs. Among the arithmetical operations allowed by ANSYS, the ones used were addition, multiplication, and exponentiation.

After the lifetime is computed for each element in the model, maximum damage is located by plotting the results from the ETABLEs, first for the solder balls, then for the copper TSVs. After plotting the results for the solder balls, the ball that contained the element with the maximum damage was chosen, and an average based on the damage in each element pertaining to that solder ball was computed. All damage was weighted equally.

Since the copper TSVs were very long and consist of many elements, the maximum damage-carrying element was located, and the closest element was chosen conjunctively with that of maximum damage to obtain the average damage. This procedure was done to avoid the influence of very-low damage-carrying elements in the long TSVs.

Minitab software was used to analyze the result of the experiment and to plot main effect diagrams. The results were normalized with respect to the first run. These results are shown in Figs. 5 and 6 for the solder joints and the TSVs, respectively. The number of elements of the solid model was approximately 53,440 elements. This mesh size was obtained by creating small sections of the whole model individually, and meshing each one of these sections to ensure elements were not distorted, and were sufficient to model the intended shape, e.g. solder balls were round and not square. Mesh sensitivity was conducted for one case by refining the mesh in solder joints and TSVs. The number of elements was increased to 93,308, and the selected mesh density was found to be sufficient as no significant change in the results was seen.

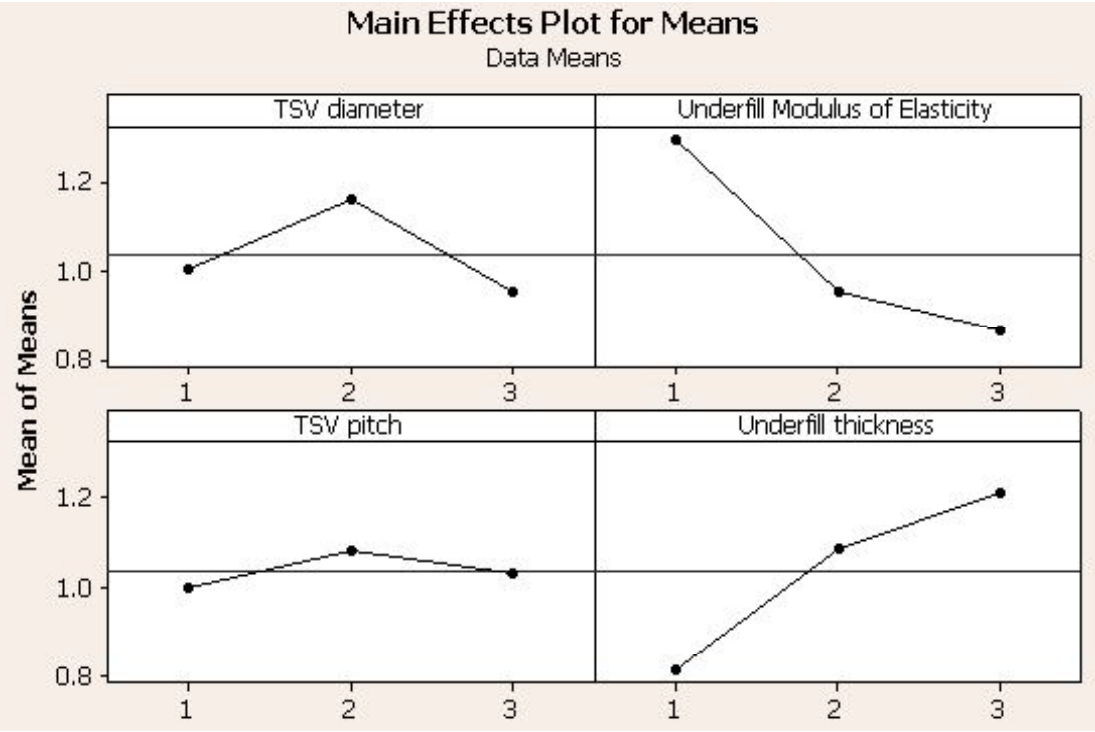

Figure 5. Main effect diagrams for solder joints durability.

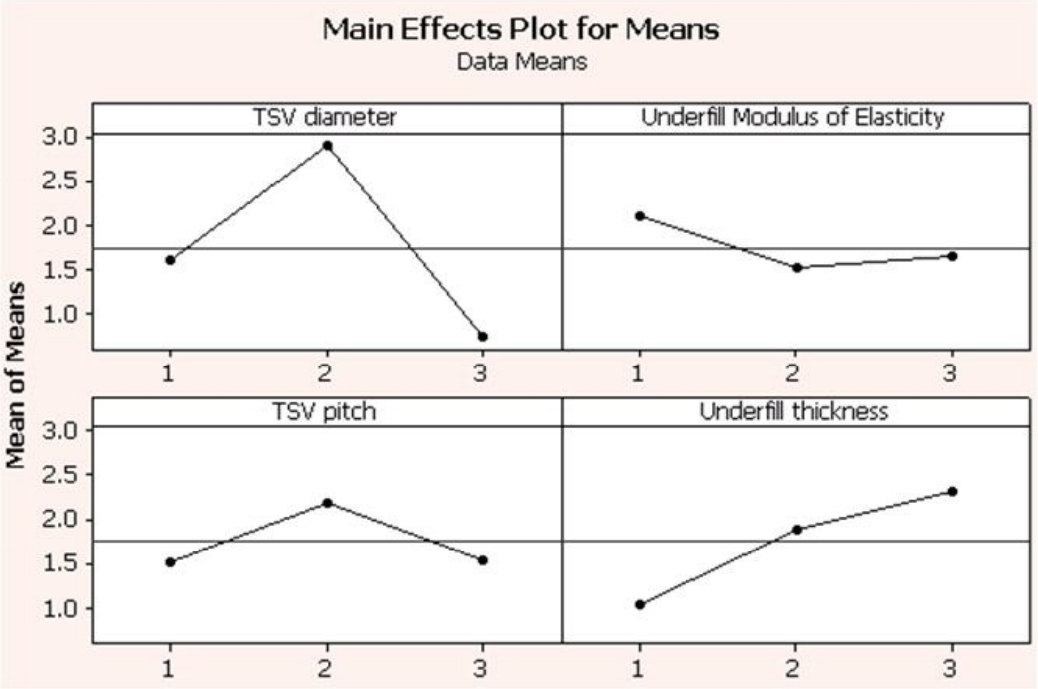

Figure 6. Main effect plots for TSV durability.

As seen on Fig. 5, main effect for solder joints durability followed a non-monotonic trend for the TSV diameter and the TSV pitch with regards to the solder joints durability. This indicates that for this specific architecture and material, the optimum level of these parameters are in the selected range. The underfill thickness and the underfill modulus of elasticity show a monotonic trend. As expected, as the underfill stiffness increases, the durability decreases. Also, as the underfill becomes stiffer, it loses the capacity to deform, thus inducing more deformation on the solder joint, resulting in increased strain energy released in the solder, and reducing the durability of the solder joints. Increasing the underfill thickness shows a monotonic increase in durability of solder joints. Underfill thickness has a direct relationship with the height of the solder. It has been shown previously that increasing solders height increases the durability [17] and is confirmed here in this study.

The same analysis was conducted for the TSV interconnects. In the case of TSV, it can be seen from Fig. 6 that the TSV diameter has a very strong effect. Reliability can be improved drastically in optimized situations where the medium level of TSV diameter is selected. The optimized level seemed to be in the selected range for all the variables except underfill thickness. Underfill thickness had the same effect on TSV as on solder joints. This can be explained by the fact that increasing the height of the joints makes the structure more compliant, inducing less stress and deformation on TSV interconnects.

Location of failures for solder joints was observed to be consistently in the solder ball in the last column of interconnects connecting the fourth layer of silicon, which is consistent with previous findings of authors indicating a failure of the joint with the longest distance from neutral point (DNP) [18]. The failure sites for TSV were also found to be in the last column of interconnects; however, it varied between layers in different runs. For runs 1 through 4, the amount of silicon material surrounding the lower TSV is large enough to cause severe damage. However, for runs 5 through 9, as the die thickness is changed from low level to nominal and high levels, the amount of silicon is increased, and now the CTE mismatch is greater for the top TSV interconnect. Locations of these failures are shown in Fig. 7.

As per definition, main effect is the effect of each parameter when other parameters are kept constant. Therefore, the main effect results show the effect of each individual parameter. The conclusions drawn here are based on single factor effect and therefore, taking the interactions into account should not change the conclusions.

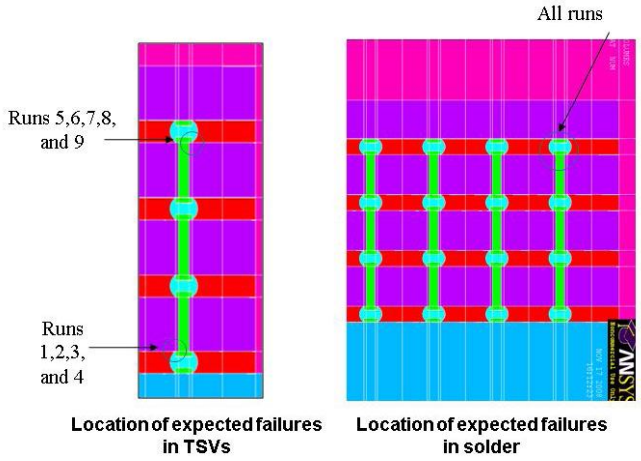

Figure 7. Location of failures for TSV copper interconnects (left) and solder joints (right).

2.7. Recommendations

From the previously drawn conclusions, the following recommendations are suggested for consideration:

- A soft underfill material, such as hexahydromethylphalic anhydride (HMPA) which has a modulus of elasticity of 2.5GPa [19] should be used for 3D ICs using DCA bonding technology.
- Since optimum values are expected within the selected range for the TSV diameter and TSV pitch, this study cannot provide the exact values for optimization. More studies should be conducted that should focus on these parameters to determine what the actual trend is within the selected range, and to be able to obtain what the real optimum values are.
- Based on the available information and for bonding technology analyzed, the die thickness and TSV diameter should be 100μm and 20μm, respectively.
- Similarly, the TSV pitch should be 95μm.

CHAPTER 3

MEASUREMENT OF STRAIN AT MICROSCOPIC SCALE UTILIZING PIEZOELECTRIC CHARACTERISTICS

3.1. Introduction and Literature Review

Strain measurement has been the subject of many studies and has been accomplished through the utilization of different methods. According to Perry on *Strain Measurements and Stress Analysis* [20], resistive strain gauges are the most widely used strain gauges in the United States, with 80 percent or more of the stress measurement experiments being performed with them. These gauges have been used to measure force, pressure, torsion, and bending [21]. A disadvantage of this method is that large strain measurements cannot be achieved, measuring at most 1 mm/m; also, ambient temperature will impact the strain readings, so a very controlled environment is required in order to achieve accurate measurements. Semiconductor strain gauges follow the same principles as resistive strain gauges; however, the resistive material is substituted by a semiconductor material, such as silicon or germanium [20]. They have a higher sensitivity to strain, and the breaking strength and elastic strain range is much higher than that of the resistive strain gauges. On the other hand, the temperature range for operation of the semiconductor strain gauges is much smaller (-40 °C to +100 °C), and its useful linear range is only ±0.5 mm/m [20] making it less appealing for high-temperature and high-resolution applications.

Photo-elasticity principles are used in strain measurement where an optical mean is utilized to determine strain. These principles apply mainly to the elastic region; however, research has been done to optically measure inelastic strain [20]. Examples of this technique include Moiré fringe patterns, photo-elastic coating, and brittle lacquer method.

Moiré fringe patterns are used in determining the strain of different types of materials [20]. They have been used to measure in-plane and out-of-plane deformation, as well as rotation and curvature. Large deformations can be measured accurately with this technique; however, for small deformation, it requires high-sensitivity moiré interferometry. Another similar method is photo-elastic coating [20]. A thin sheet of photo-elastic material is bonded to the material being analyzed; as it is loaded, the coating will deform, and a strain field is developed in the coating. It is non-destructive and directly measures the strain in the material. A different photo-elastic method to determine the strain distribution is the brittle lacquer method [22]. Lacquer is a varnish used to coat the structure where the strain field is being measured. Under tensile stress it breaks easily, and the crack pattern is analyzed. The spacing of the cracks indicates the amount of local strain the structure is subjected to. This method requires a calibration strip to compare the strain field to, which introduces errors from indirect measurement.

X-ray diffraction has also been used in strain measurement [22]. It consists of applying X-rays to the structure where the strain is to be measured. From the reflected pattern, the stresses can be determined. It requires the wavelength of the incident X-rays be of comparable size to the atomic spacing in a crystal. Also, this type of measurement only helps in determining the elastic strain and can only be employed in the crystal orientations that can produce X-ray diffraction.

Acoustic strain gauges [22] consist of a main strain gauge attached to a steel wire that is plucked by means of a magnet in order to read the natural frequency of the wire. A disadvantage to this type of gauge is that the tension forces on the wire are not taken into consideration and will impact the outcome.

Pneumatic strain gauges use the principle of a pressure increase due to restricting the flow stream [22]. This method is very accurate in the measurement of static and dynamic strain; however, an extensometer is employed to visualize the strain which is very nonlinear and thus requires more complicated configurations to reduce this nonlinearity.

Uttam et al. [23] utilized optical fiber to measure strains in the order of magnitude from 0.1 μm/m up to 1000 μm/m. The advantages of this system include a wide range of microstrain measured with high accordance with respect to resistive strain gauges, and a higher operating life than resistive strain gauges. Conversely, in order to use this method, the optical fiber has to be embedded in the specimen being measured, demodulation circuitry has to be employed, and signal comparison has to take place to determine strain.

Chu et al. [24] achieved microstrain measurements by means of differential capacitive strain sensors. The capacitive sensors are fastened to ribs which are attached to the beam where the strain is measured. The residual strain will produce an inward or outward motion that will change the capacitance in the sensors and by determining the difference, a strain can be calculated. Although not primarily intended for measuring strain, the obtained results were utilized to determine coefficients of thermal expansion, and the values were within specifications with respect to prior measurements. Other use for this differential capacitive sensor includes measurement of modulus of elasticity.

Another method that has been studied is measurement through the utilization of a magnetoelastic microtransformer. This approach was taken by Amor et al. at the Institute for Microtechnology, Hanover University in Germany [25]. They utilized a magnetoelastic material in order to take advantage of the Villari effect. The Villari effect is such that the stress applied to a magnetoelastic material will in turn change its permeability. Measurements have been made of the intensity of magnetization and the magnetizing force

for different rods, one rod under tension and the other one with no force applied [26]. The point of intersection between these two curves is the Villari critical point, at which the force applied on the material does not change the permeability. This is the inverse effect of the magnetostriction discovered by James P. Joule. A microtransformer made out of NiFe was built and attached to a silicon beam in order to perform the measurements. As the beam was subjected to a lateral force, the permeability of the microtransformer changed. After obtaining a characteristic curve for the NiFe specimen between the applied stress and the normalized change in the relative permeability, the strain was determined. Only compressive strains were reported in the work. Another research on magnetoelatic microtransformers was conducted by a joint team of researchers from the Slovak University of Technology, the Institute of Physics in the Czech Republic and Slovakia and the Istituto Elettrotecnico Nazionale Galileo Ferraris in Italy, where they determined the effect of ambient temperature on the strain measurements [27]. They concluded that for a strain sensor mounted on a substrate using glue the effect of temperature is significant, especially compared to the same sensor not attached to a substrate.

At the microscopic scale, several of the aforementioned methods cannot be utilized due to a reduced precision at such levels. For this reason, a new technique is proposed for measuring tensile and compressive strains particularly applicable to the microscopic scale using piezoelectric materials [28].

3.2. Device Architecture and Principle of Function

The proposed apparatus consists of two piezoelectric members that constrain the specimen being tested from both sides [29]. The piezoelectric members are constrained within a very rigid frame as seen in Fig. 8. One of the piezoelectric materials will act as a load cell, and it will have a voltage applied to it. The second piezoelectric material will act as a

strain sensor and it will have leads that will be connected to a voltmeter to read an output voltage.

Accuracy on the system will depend on obtaining a sufficiently stiff frame that will experience strain relatively negligible compared to the strain the piezoelectric materials and the test material will experience. A soft frame would deform as the voltage is applied to the piezoelectric material, then this deformation would have to be taken into account for the total strain of the system. Therefore, the output voltage from the piezoelectric material would determine the sum of the deformation of the test material, the piezoelectric materials, and the frame together; resulting in an undetermined system of equation. Another characteristic of the frame is that it has to be completely insulated; this will ensure that no short circuit would occur as the voltage is applied, which could result in harming the system, or, more importantly, the operator.

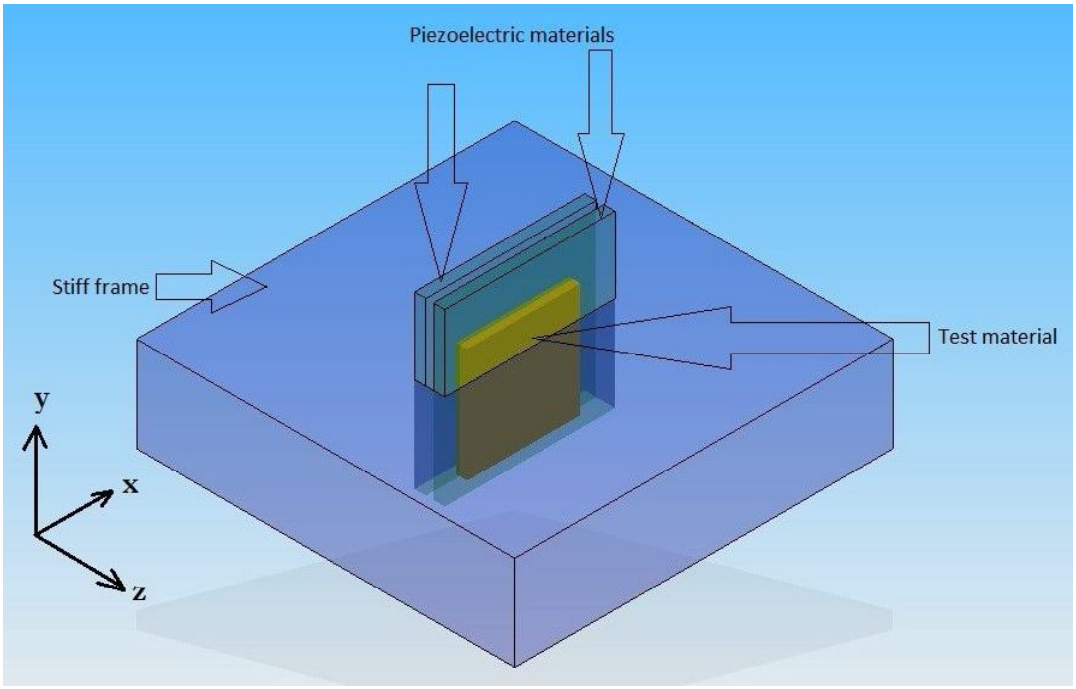

Figure 8. Schematic representation of the strain measuring system.

As the input voltage is applied on the first piezoelectric member, it deforms. Since the structure is constrained within the rigid frame, the algebraic sum of the deformation of the piezoelectric members and specimen is approximately zero along the thickness direction, or z-direction. Depending on the stiffness of the test specimen, a force is developed in the first piezoelectric member that is transferred to the second piezoelectric member and induces deformation in the second piezoelectric member. This deformation can be determined through measuring the output voltage signal. Utilizing the piezoelectricity principle that states there is a linear relation between deformation and electric field, the strain is readily obtained.

For a material undergoing plastic deformation, the same principle is utilized. The output voltage in the output piezoelectric material will be governed by the stress-strain curve of the test specimen. Therefore, the stress-strain curve for different test specimens can be obtained. The theory behind the proposed device is given below.

3.3. Theoretical Analysis

Piezoelectricity is a linear phenomenon that relates linear elasticity with the electric charge equations through the use of the piezoelectric constants [30]. Many applications have been developed for the use of piezoelectric materials, including acoustic emission detectors, medical ultrasonic transducers, piezoelectric actuators and buzzers, and piezoelectric transformers supplying high voltage [31].

The governing equations for piezoelectricity in matrix form are

$$\vec{T} = [c_e] \cdot \vec{\varepsilon} - [e] \cdot \vec{E}, \tag{9a}$$

$$\vec{D} = [e] \cdot \vec{\varepsilon} + [\pi_S] \cdot \vec{E}, \tag{9b}$$

where the square brackets refer to properties matrices. T and D are the stress and electric displacement, respectively, ε and E are the strain and electric field, respectively, and c_E, e and π_S are the stiffness, piezoelectric and dielectric constant matrices, respectively. The subscripts E and S stand for constant or zero electric field and constant or zero strain, respectively. The stress, T, and strain, ε, column vectors are composed of six components, three axial and three shear. The electric displacement, D, and electric field, E, only contain three axial elements each. The elastic constant c_E is a 6x6 symmetric matrix; the dielectric constant π_S is a 3x3 diagonal matrix; and the piezoelectric constant e is a 3x6 matrix. More commonly, the elastic compliance s_E and the piezoelectric strain constant d are provided by the manufacturers instead of c_E and e, and they have to be transformed to the form of Eq. (9) in order to be utilized by a finite element analysis tool such as ANSYS. Such transformations are defined as [31]

$$[s_E] = [c_e]^{-1}, \tag{10a}$$

$$[d] = [e] \cdot [s_E]. \tag{10b}$$

According to the crystal structure of the piezoelectric material, the material property constants have been determined to show symmetry that reduces the number of independent constants in each material matrix. A positive orientation for a piezoelectric material is such that the piezoelectric constant is positive, so the right-hand rule does not uniquely determine the crystallographic axis orientation [31].

As part of the 4mm crystal class, lead zirconate titanate (PZT) is a piezoelectric ceramic that exhibits great deformation when subjected to an electric field. Its crystal structure is such that the x- and y-axes are symmetric reducing the number of material constants to only two thirds of the total number of constants. From the wide range of PZT ceramics, PZT-5H, commonly known also as Navy VI, was chosen due to its high d_{33} value,

which means the material will have greater deformation in the direction of the applied electric field than any other material for the same applied voltage.

In order to achieve strain measurement, an isotropic test specimen is placed between the PZT piezoelectric materials that will be fixed at both ends from displacement. One of the piezoelectric materials is placed under inverse piezoelectric polarization (an electric field is applied to it that will induce mechanical deformation); this PZT will be referred to as PZ1. The other one will then be deformed resulting in an induced electric field that will be measured by means of a voltmeter (direct piezoelectric polarization); this PZT will be referred to as PZ2. The applied voltage on PZ1 will induce an electric field of magnitude

$$E_i = {}^{dV}/_{dx} = {}^{V_i}/_{t}, \tag{11}$$

where V_i is the input voltage, and t is the thickness of PZ1. The algebraic sum of the deformations along the polarization direction (z-direction) must be zero. Mathematically, we have,

$$\Delta l_{z1} + \Delta l_{z2} + \Delta l_{z3} = 0, \tag{12}$$

where the subscripts 1, 2 and 3 refer to PZ1, the test specimen, and PZ2, respectively. The original thickness t is assumed equal for the three components. Dividing Eq. (12) by t, strain is calculated as

$$\varepsilon_{z1} + \varepsilon_{z2} + \varepsilon_{z3} = 0. \tag{13}$$

PZ1 is subjected to traction and the applied electric field; hence, by superimposing the strain due to each of these phenomena, the strain is $\overrightarrow{\varepsilon_1} = [d]^T \cdot \overrightarrow{E_i} + [s_E] \cdot \vec{T}$; PZ2 is also subjected to traction; however, no electric field is applied to it, and so the strain in PZ2 is $\overrightarrow{\varepsilon_3} = [s_E] \cdot \vec{T}$. The strain in the test material is given by Hooke's law as $\overrightarrow{\varepsilon_2} = [E]^{-1} \cdot \vec{T}$. Substituting the strains back into Eq. (13), traction can be solved for as follows.

$$T_1 = -\frac{d_{33}\cdot E_i}{2s_{E33}+\frac{1}{E}} = -\frac{d_{33}\cdot V_i}{t\left(2s_{E33}+\frac{1}{E}\right)}, \quad (14)$$

After obtaining the strain experienced by each material, the electric field on PZ2 is computed in order to determine the output voltage V_o. Using the principle of the direct piezoelectric effect, the electric field is determined as

$$\overrightarrow{E_o} = -[h]\cdot\overrightarrow{\varepsilon_3}, \quad (15)$$

where $[h] = [g]\cdot[s_D]^{-1}$, and $[g] = [\pi_T]^{-1}\cdot[d]$ and $[s_D] = [s_E] - [d]^t\cdot[\pi_T]^{-1}\cdot[d]$, a piezoelectric stress constant [30]. Ultimately the output voltage is obtained as

$$V_o = E_o\cdot t. \quad (16)$$

Alternatively, given the applied voltage V_i and the measured output voltage V_o, the modulus of elasticity of the test specimen can be computed. Parting from Eq. (13), we solve for ε_{2z} resulting in

$$\varepsilon_{2z} = -(\varepsilon_{1z} + \varepsilon_{3z}). \quad (17)$$

Rewriting the strain equations in the z-direction, the resulting equations are $\varepsilon_{1z} = d_{33}\cdot E_i + s_{E33}\cdot T_1$, $\varepsilon_{2z} = \frac{T_1}{E}$, and $\varepsilon_{3z} = s_{E33}\cdot T_1$. Substituting into Eq. (17) and solving for the modulus of elasticity, E, the final expression becomes

$$E = \frac{T_1}{-(d_{33}\cdot E_i + 2s_{E33}\cdot T_1)}, \quad (18)$$

where the traction T_1 is given by $T_1 = \frac{\varepsilon_{3z}}{s_{E33}} = \frac{d_{33}\cdot E_o}{s_{E33}}$.

3.4. Finite Element Simulation

A finite element model is built in ANSYS to corroborate the theoretical results, to determine the effect of the specimen and the piezoelectric materials thicknesses, and to analyze how the permeability of the test specimen may influence the strain measurement.

Additionally, plastic deformation is also studied to determine the behavior of the output voltage as a function of the plasticity.

To perform the finite element analysis (FEA), element SOLID5 is selected as it is a coupled-field solid with capabilities in thermal, magnetic, electrical, structural and piezoelectric analysis. In this study, only the structural and piezoelectric capabilities are of interest. In Fig. 9 the created solid model is described, as well as the boundary conditions and the orientation of the coordinate axes. The boundary conditions are represented by the different colored arrows; the green arrows represent the voltage degrees of freedom (DOF), and the blue arrows represent the displacement DOF.

Given the problem description, the leftmost area for PZ2 and the rightmost area for PZ1 have been constrained with no motion. The rightmost area for PZ2 and the leftmost area for PZ1 are grounded to ensure no voltage drop will occur across the test specimen. The input voltage of the system is applied on the rightmost area of PZ1. The input voltage is changed accordingly at each load step whereas the remaining DOFs stayed unchanged.

For an initial test, the test specimen is treated as an elastic material, i.e. no plasticity is considered. The material properties are detailed in Table 5. The voltage is applied to PZ1 from 0v to 60v in increments of 10v at each load step.

Properties of the test material are changed at the second stage in order to introduce plasticity into the system, and the voltage levels are varied such that the test material deforms plastically. SOLID5 does not have outputs of plasticity; therefore, the test specimen is modeled using SOLID185 that can model plasticity while the piezoelectric materials remained as SOLID5. Plasticity in the test specimen is modeled as experiencing a bilinear isotropic hardening behavior, the material properties are listed in Table 6. The input voltage was changed from 0v to 250v with increments of 25v at each load step.

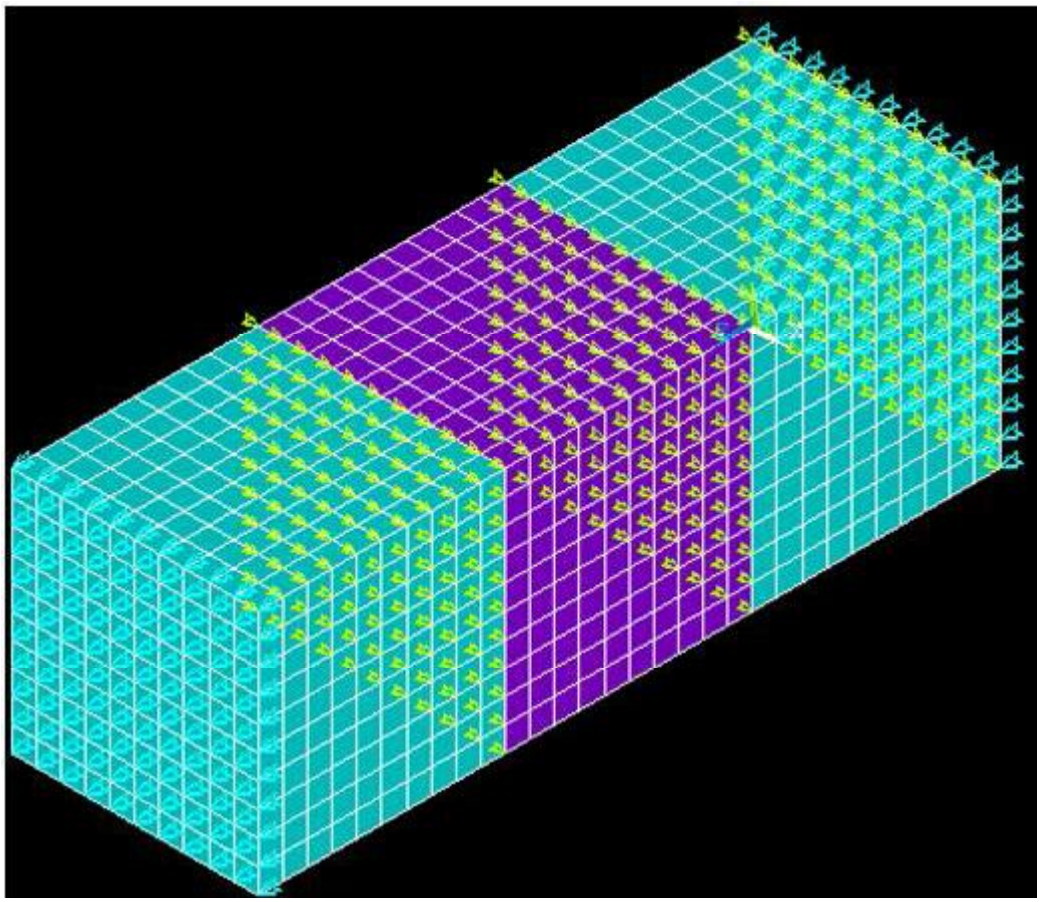

Figure 9. 3D finite element model of strain measuring system.

Table 5. Material Properties of Test Specimen for FEA

Property	Magnitude
Modulus of elasticity	15.792 GPa
Poisson's ratio	0.3

Table 6. Material Properties of Plastic Test Specimen for FEA

Property	Magnitude
Modulus of elasticity	15.792 GPa
Poisson's ratio	0.3
Yield stress	91.5 MPa
Tangent modulus	0.5171 kPa

The properties for PZT-5H for the theoretical analysis and for the finite element modeling are as follow

$$[d] = \begin{bmatrix} 0 & 0 & 0 & 0 & 741 & 0 \\ 0 & 0 & 0 & 741 & 0 & 0 \\ -274 & -274 & 593 & 0 & 0 & 0 \end{bmatrix} \times 10^{-12}\, {}^{C}/_{N} \tag{19a}$$

$$[s_E] = \begin{bmatrix} 16.5 & -4.78 & -8.45 & 0 & 0 & 0 \\ -4.78 & 16.5 & -8.45 & 0 & 0 & 0 \\ -8.45 & -8.45 & 20.70 & 0 & 0 & 0 \\ 0 & 0 & 0 & 43.5 & 0 & 0 \\ 0 & 0 & 0 & 0 & 43.5 & 0 \\ 0 & 0 & 0 & 0 & 0 & 42.5 \end{bmatrix} \times 10^{-12}\, {}^{m^2}/_{N} \tag{19b}$$

$$[\pi_T]/_{\pi_0} = \begin{bmatrix} 3130 & 0 & 0 \\ 0 & 3130 & 0 \\ 0 & 0 & 3400 \end{bmatrix} \tag{19c}$$

where the permittivity of free space $\pi_0 = 8.854 \times 10^{-12}\, {}^{F}/_{m}$ and the subscript *T* stands for constant or zero stress field. The relationship between π_E and π_T is given by [31]

$$[\pi_E] = [\pi_T] + [d] \cdot [e]. \tag{20}$$

3.5. Characteristic Curve

Prior to utilizing the PZT, it is necessary to understand how it will behave under the conditions prescribed by the strain measurement system. For this reason, characteristic curves are plotted to determine the trend of the input voltage as a function of the output voltage for different moduli of elasticity of the test specimen. In order to achieve this, the traction equation, Eq. (14) is substituted into the strain relationship for PZ2, i.e. $\overrightarrow{\varepsilon_3} = [s_E] \cdot \vec{T}$, so that

$$\varepsilon_{3z} = s_{E33} \cdot \frac{d_{33} E_i}{2 s_{E33} + {}^{1}/_{E}}. \tag{21}$$

From Eq. (15) an expression relating the output and input electric fields in terms of the modulus of elasticity of the test specimen is written, i.e.

$$E_o = -h_{33} \cdot \left(s_{E33} \cdot \frac{d_{33} E_i}{2 s_{E33} + {}^{1}/_{E}} \right), \tag{22}$$

or, in terms of voltage drops, and assuming the same thickness,

$$V_o = -h_{33} \cdot \left(s_{E33} \cdot \frac{d_{33} V_i}{2 s_{E33} + {}^{1}/_{E}} \right). \tag{23}$$

Starting with Eq. (23), the output voltage as a function of the input voltage is plotted, changing the modulus of elasticity from 200MPa up to 900MPa with increments of 100MPa on Fig. 10, and from 1GPa up to 100GPa with increments of 10GPa on Fig. 11.

It is observed on Fig. 11 that as the modulus of elasticity of the test specimen increases, the characteristic curves fall closer together. From Eq. 23, as the modulus of elasticity of the test specimen is increased, its inverse may become comparatively zero compared to $2s_{E33}$, and its effect then becomes negligible. For this reason, careful attention has to be paid in order to avoid getting erroneous data.

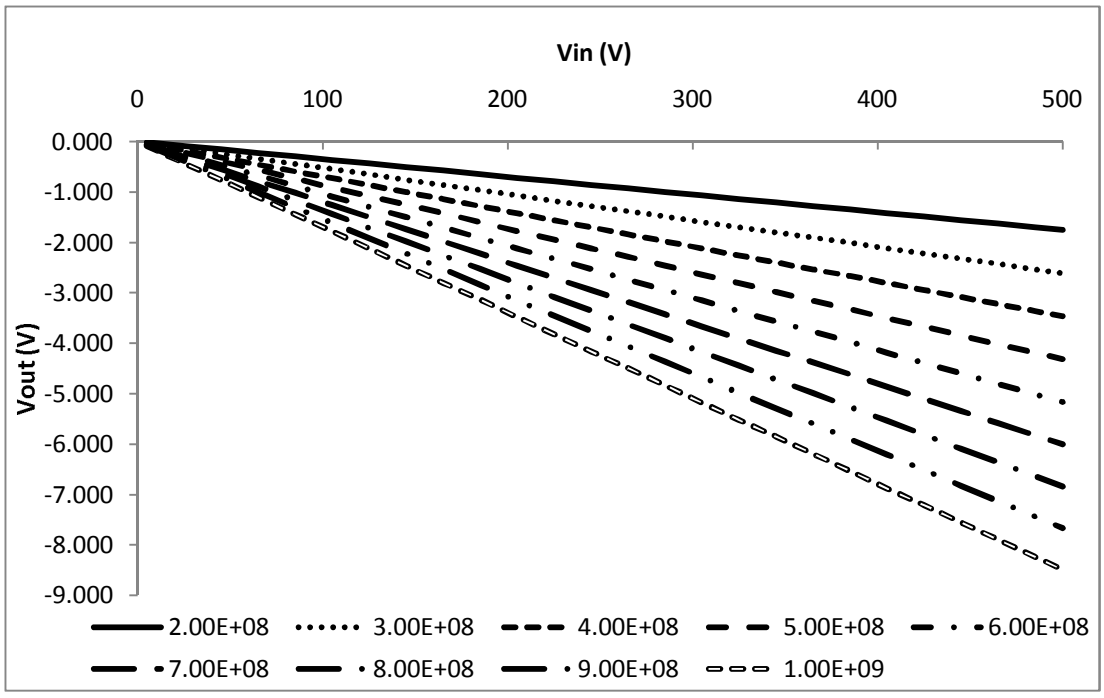

Figure 10. Output vs. input voltage at constant test specimen modulus of elasticity (200MPa to 1GPa).

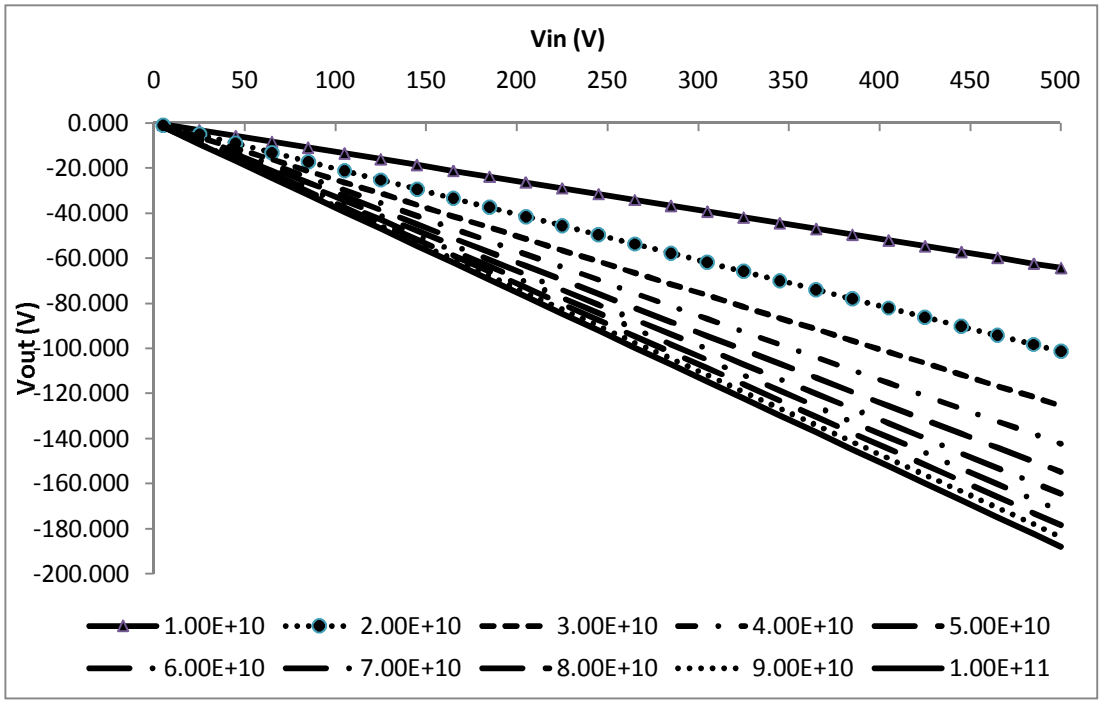

Figure 11. Output vs. input voltage at constant test specimen modulus of elasticity (10GPa to 100GPa).

3.6. Nonlinear Behavior

As the input voltage is augmented and the traction increases, the test specimen may undergo plastic deformation, i.e. the yield strength may be excited, which translates into permanent deformation of the test specimen. Ideally, plastic deformation can behave in different manners; perfectly plastic, bilinear isotropic hardening, bilinear kinematic hardening, multilinear isotropic hardening, and multilinear kinematic hardening are a few examples of the different models for plasticity.

For this analysis a bilinear isotropic hardening behavior for the test specimen is assumed. On Fig. 12 the stress-strain curve for such a material is plotted. At an initial stage, the material behaves elastically, with a slope equal to the modulus of elasticity. After reaching the yield stress of the material, the specimen starts to behave plastically yet still linearly. The slope of the curve now changes to the tangent modulus.

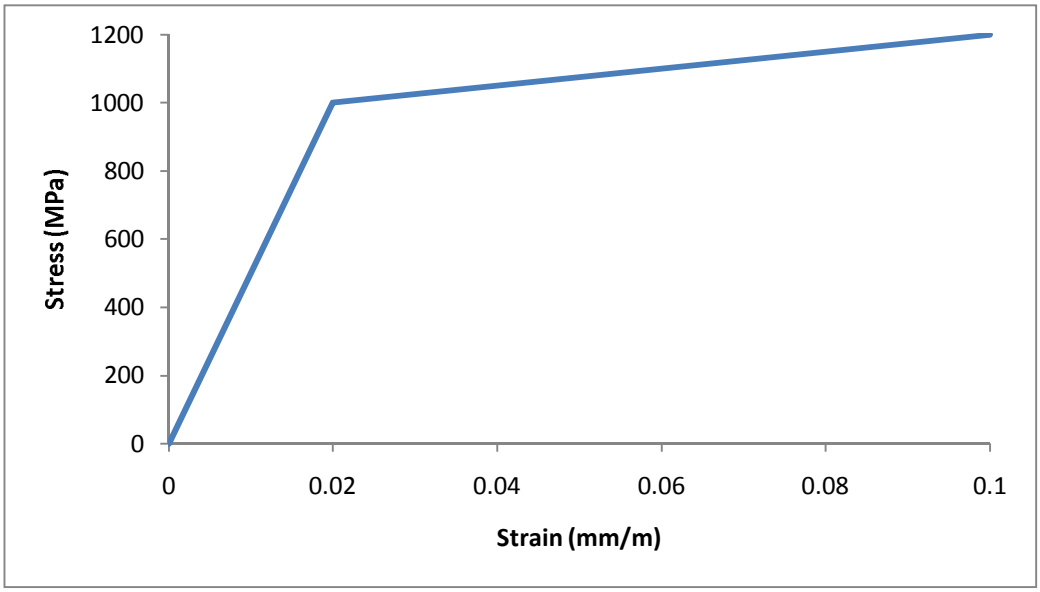

Figure 12. Stress-strain curve for a material experiencing bilinear isotropic hardening.

After the test specimen yields, the traction of the system is governed by stress of the test specimen. The equation of the stress as a function of strain after yielding is given by

$$\sigma(\varepsilon) = \left(1 - \frac{E_p}{E}\right)\sigma_Y + E_p \cdot \varepsilon, \varepsilon \geq \frac{\sigma_Y}{E}, \tag{24}$$

where σ is the stress and ε is the strain in the test material, E is the modulus of elasticity, E_p is the tangent modulus and σ_Y is the yield strength. Through the piezoelectric relations, since the traction is equal in all three materials, then the strain in PZ2 is given by

$$\varepsilon_{3z} = s_{E33} \cdot \sigma(\varepsilon_{2z}), \tag{25}$$

and the output voltage is obtained similarly as before by applying Eqs. (15) and (16).

3.7. Results and Conclusions

The finite element method results are compared with the theoretical values computed for the case where the test specimen was assumed to behave strictly elastic. Table 7 summarizes the strain of the test specimen, the output voltage and the traction of the

system per run, and a percentage difference was calculated. Due to simplifications in the theoretical analysis, the finite element results were taken as exact.

In analyzing the data from the finite element model, an average of the stresses and of the strains over the entire volume was computed; for the voltage, an average of the voltage on the polarized xy-faces of PZ2 was taken and the voltage drop is computed as the difference between the two faces' voltages. Additionally, the average was computed using only the nodes along the centerline of the model; however, the results did not show any significant change, and hence were not taken into consideration.

We observe from the percentage differences on Table 7 that the finite element model predicts with relative accuracy the strain on the test specimen and the system traction; however, the output voltage on PZ2 has a higher difference associated with it between the analytical results and the finite element results. This discrepancy can be attributed to assuming the electric field will be constant throughout the piezoelectric materials; however, the change in shape of the material will make the differential Eq. (11) be non-constant, and a more accurate expression for the voltage drop across the piezoelectric materials would be needed. As a preliminary study, it proves the feasibility of the system of relating the test specimen strain to the output voltage. Also, the analytical study does not take into consideration the effect of Poisson's ratio as the materials start deforming, only traction along the polarized direction is considered. As the material shrinks, the thickness is decreased and by Eq. (11) it is predicted that the voltage induced will be smaller.

Table 7. FEA Results vs. Analytical Results Comparison

V_{in}	Test specimen strain (μm/m)			Output voltage (v)			System traction (kPa)		
	FEA	Analytical	%Error	FEA	Analytical	%Error	FEA	Analytical	%Error
10v	-0.56	-0.72	-22.2	-1.34	-2.15	-37.7	-13.4	-11.3	18.6
20v	-1.12	-1.43	-21.7	-2.68	-4.30	-37.7	-26.7	-22.7	17.6
30v	-1.68	-2.15	-21.9	-4.02	-6.44	-37.6	-40.0	-34.0	17.6
40v	-2.24	-2.87	-22.0	-5.35	-8.59	-37.7	-53.4	-45.3	17.9
50v	-2.79	-3.59	-22.3	-6.69	-10.7	-37.5	-66.8	-56.6	18.0
60v	-3.35	-4.30	-22.1	-8.02	-12.9	-37.8	-80.1	-68.0	17.8

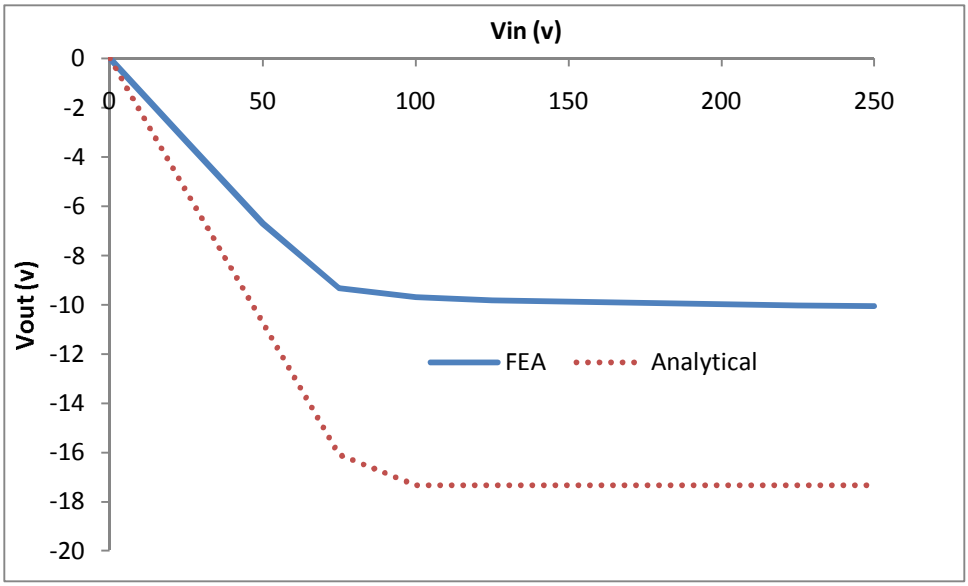

Figure 13. Output voltage of FEA and analytical analysis with plastic test specimen.

For the plastic test specimen, the output voltage as a function of the input voltage is plotted on Fig. 13 for both the finite element method results and the analytical results. The finite element results predict lower voltage values as per the same reasons as described for the elastic test specimen case. It is observed how both plots follow the expected behavior of plasticity.

For these finite element results, the test specimen was assumed to have zero permeability, which means that no electric field can be induced inside the material. Another test was conducted assuming a relative permittivity of 3,130, and the results showed no difference. This was due to the fact that the test specimen was grounded at both ends, which short-circuited it and did not allow any voltage variation inside it.

On another trial, the thicknesses of the piezoelectric materials were doubled, and the thickness of the test specimen remained constant. In Table 8, the finite element results for the same thickness and the changed thickness are compared. The stresses and the strains have decreased whereas the output voltage increased.

For the thicker piezoelectric materials, the governing equation becomes

$$2\varepsilon_{z1} + \varepsilon_{z2} + 2\varepsilon_{z3} = 0, \tag{26}$$

and solving similarly to the procedure in section 3.3, the traction of the system becomes

$$T_1 = -\frac{d_{33}\cdot E_i}{2s_{E33}+\frac{1}{2E}} = -\frac{d_{33}\cdot V_i}{t\left(4s_{E33}+\frac{1}{E}\right)}, \tag{27}$$

The denominator in Eq. (27) is larger than that of Eq. (14) which results in a lower system traction, and by $\overrightarrow{\varepsilon_3} = [s_E]\cdot\vec{T}$ then the strain in PZ2 is also lower. The output voltage is similar to Eq. (16), however, with the thickness doubled, it becomes

$$V_o = 2E_o \cdot t, \tag{28}$$

and since the traction is reduced by less than half its value with the same thickness in all three materials, then the output voltage is higher than the case with equal thicknesses. Higher voltage levels for lower strain helps to achieve smaller strain measurements and to still have measurable voltage levels at the output.

A microstrain measurement device was proposed with the purpose of achieving accurate measurements using piezoelectricity. A finite element model was created on ANSYS to compare the results with the analytical approach. The stress and strain values showed similarity with differences ranging between 17% and 23% with respect to the analytical result. The differences computed for the output voltage were, however, between 37% and 38%. These differences in value may be attributed to the simplification in the analytical approach to not take into consideration the Poisson's ratio of the materials and also to assume the electric field inside the piezoelectric materials to be constant throughout. Testing for a material that will undergo plastic deformation was proven to be feasible with this device, as it was observed on Fig. 13 how the output voltage reflected the nonlinearity of the stress-strain curve.

Table 8. Comparison of Measured Values for Same and Different Thickness

Vin (v)	Stress (kPa)		Strain (μm/m)		Output voltage (v)	
	Same t	Different t	Same t	Different t	Same t	Different t
10	-13.4	-9.92	-0.56	-0.45	-1.34	-1.98
20	-26.7	-19.83	-1.12	-0.9	-2.68	-3.96
30	-40	-29.74	-1.68	-1.36	-4.02	-5.93

3.8. Recommendations

As the idea is taken to the building stage, the following recommendations are made in order to ensure safety and the correct functioning of the device. This guideline is not intended to be a full list of the topics to be considered.

The piezoelectric materials have to be completely isolated on all sides to avoid the electric field of one piezoelectric material from affecting the other one.

The breakdown voltage of a piezoelectric material refers to the maximum voltage level that the material will withstand before becoming an electric conductor [32]. The breakdown voltage of PZT is approximately 600kv/cm [33], which means that for piezoelectric materials with thickness of 1μm, the maximum voltage that can be applied is 60v.

To achieve tension measurements, all three materials would have to be bonded together, and the polarization of PZ1 changed, which would compress it. The test material, and PZ2 will have to expand. Theoretically, the analysis is the same. In reality, the stress of the adhesive material has to be taken into consideration, and the finite element model has to be modified to include contact elements.

CHAPTER 4

SUMMARY AND CONCLUSIONS

Three-dimensional integrated circuits (3D ICs) have been designed with the purpose of achieving higher communication speed by reducing the interconnect length between integrated circuits, and integrating heterogeneous functions into one single package. Numerical analysis of effect of different design parameters on thermo-mechanical durability of TSV copper interconnects and SAC solder joints was conducted using finite element modeling. These parameters included the TSV pitch, TSV diameter, underfill stiffness, and underfill thickness. A three-level Taguchi design of experiment method was utilized to evaluate the effect of each parameter. A three-dimensional finite element model was built in ANSYS to analyze the effect of these parameters under thermo cyclic loading. The package was subjected to thermal cyclic loading, and the stresses and damage in the interconnects were evaluated using Coffin-Manson fatigue damage and energy partitioning damage models.

Solder ball reliability was more influenced by the underfill modulus of elasticity; whereas the TSV pitch has the least amount of effect. An increase in underfill thickness translated into an increase in the overall life of the 3D IC in terms of the solder ball reliability. TSV reliability was more influenced by TSV diameter. The failures of both solder and TSV, for all the cases, were located in the last row of the joints. Mesh sensitivity was conducted for one case by refining the mesh in solder joints and TSVs, and the selected mesh density was found to be sufficient as no significant change in the results was seen.

A microstrain measurement device was also proposed with the purpose of achieving accurate measurements using piezoelectricity. Advantages of the proposed system include ease of use particularly at microscopic scale, adaptability to measure the strain of different materials, and flexibility to measure the modulus of elasticity for unknown materials. A finite

element model was created in ANSYS to compare the results with the analytical approach. The stress and strain values showed similarity with errors ranging between 17% and 23% with respect to the analytical result. The error computed for the output voltage was, however, between 49% and 50%. This difference in value may be attributed to the simplification in the analytical approach in not taking into consideration the Poisson's ratio of the materials and also the electric field inside the piezoelectric materials was assumed constant throughout. Plastically deformed materials were proven to change the output voltage behavior to a nonlinear curve, showing the same behavior as the stress-strain curve for the plastic material.

CHAPTER 5

CONTRIBUTIONS

The contributions this work presented to the Engineering discipline include:

- The analysis of the durability of solder joints and copper TSV joints in 3D ICs due to thermally-induced stresses.
- The localization of the sites of maximum stress in 3D ICs with direct chip attach (DCA) bonding technology under thermo-mechanical loading.
- The proposal of a new methodology of measuring strain at the microscopic scale using the principle of piezoelectricity.
- The determination of an innovative way of calculating the modulus of elasticity of a test material.

CHAPTER 6

FUTURE WORK

Future investigations should follow the next guidelines:

- Different interconnect technologies should be studied and the results compared to these presented here in order to determine their feasibility.
- A more comprehensive study of the effect of the aspect ratio should be performed to determine how the ratio of die thickness to TSV diameter will impact the durability of 3D ICs.
- Real-time testing of 3D ICs with different number of die layers should be done to determine the effect of the number of dies in the overall cycles to failure of 3D ICs, and in the location of maximum damage.
- A study of the effect of the ratio of different material properties should be carried out where these ratios would be the factors in a Taguchi test matrix, e.g. the ratio of underfill modulus of elasticity to die modulus of elasticity
- A detailed study of the material properties of PZT should be done to assess its yield strength and the effect of plasticity in the piezoelectric behavior of the material, as well as to determine other limiting piezoelectric properties such as breakdown voltage.
- Parting from the finite element analysis results and the theoretical results, a more rigorous design of the microstrain measurement device should be done that should minimize the effect of the frame and hence reduce the error, and the required components should be purchased. Included in these components should be a high-sensitivity voltmeter.
- Different SN curves should be generated for different types of test specimens and each curve should be compared with others readily accepted as good.

REFERENCES

[1] Beyne, E., and Swinnen, B., 2007, "3D System Integration," IEEE, *International Conference on IC Design and Technology*, ICICDT 2007.

[2] Wook, S. Yo., Witarsa, D., Lim, S.Y.M., Ganesh, V., Viswanath, A.G.K., Chai, T.C., Navas, K.O., and Kripesh, V., 2006, "Reliability Studies of a Through Via Silicon Stacked Module for 3D Microsystem Packaging," *Electronic Components and Technology Conference*, pp. 1449-1453.

[3] Andry, P.S., Tsang, C., Sprogie, E., Patel, C., Wright, S.L., Webb, B.C., Buchwalter, L.P., Manzer, D., Horton, R., Polastre, R., and Knickerbocker, J., 2006, "CMOS-Compatible Process for Fabricating Electrical Through Silicon Vias," RC23867 (W0602-049).

[4] Shekhar, B., 2008, "3D technology a system perspective," Intel Corp.

[5] Bloomfield, M.O., Bentz, D.N., Lu, J.Q., Gutmann, R.J., and Cale, T.S., 2007, "Thermally Induced Stresses in 3D-IC Inter-wafer Interconnects: A Combined Grain-Continuum and Continuum Approach," *Microelectronic Engr.*, **84**, pp. 2750–2756.

[6] Zhang, J., Bloomfield, M.O., Lu, J.Q., Gutmann, R.J., and Cale, T.S., 2005, "Thermal Stresses in 3D IC Inter-wafer Interconnects," *Microelectronic Engr.*, **82**, pp. 534–547.

[7] Khan, N., Rao, V.S., Lim, S., We, H.S., Lee, V., Wu, Z.X., Rui, Y., Ebin, L.,Chai, T.C., Kripesh, V., and Lau, J., 2008, "Development of 3D Silicon Module with TSV for System in Packaging," *2008 Electronic Components and Tech. Conf.*, Lake Buena Vista, Florida, pp. 550-5.

[8] Hsieh, M.C., and Yu, C.K., 2008, "Thermo-mechanical Simulations for 4-layer Stacked IC Packages," *9th. Int. Conf. on Thermal, Mechanical and Multiphysics Simulation and Experiments in Micro-Electronics and Micro-Systems*, EuroSimE 2008, Germany.

[9] Markiewicz, P., 2009, "Computer Hardware." Retrieved: April 20, 2010, http://www.plyojump.com/classes/images/hardware/chips_completed.jpg.

[10] 2007, "Nanotechnology & Microsystems." Retrieved: April 20, 2010, http://www.mina.ubc.ca/ugrad-nanomicro-option/moreinfo_files/image011.jpg.

[11] ANSYS® Academic Research, Release 11.0, Help System, "SOLID185: 3-D 8-Node Structural Solid or Layered Solid," ANSYS, Inc.

[12] Dasgupta, A., Oyan, C., Barker, D., and Pecht, M., 1992, "Solder Creep-Fatigue Analysis by an Energy-Partitioning Approach," *J. Electronic Packaging*, **114**, pp. 152-160.

[13] Zhang, Q., and Dasgupta, A., 2005, "Systematic Study on Thermo-Mechanical Durability of Pb-Free Assemblies: Experiments and FE Analysis," *Trans. ASME J. Electronic Packaging*, **127**(4), pp. 415-429.

[14] Low, T.H., Pang, J.H.L., Lin, C.W.C., Chiang, S.C.L., and Yang, T.K.A, 2003, "Modeling Plated Copper Interconnections in a Bumpless Flip Chip Package," 2003 *Electronics Packaging Technology Conference*, Singapore, pp.791-796.

[15] Garofalo, F., 1965, *Fundamentals of Creep and Creep-Rupture in Metals,* Macmillan, New York.

[16] Taguchi, G., 1993, *Taguchi Methods: Design of Experiment.* Quality Engineering series, American Supplier Institute, Tokyo, Japan.

[17] Engelmaier, W., 1983, "Fatigue Life of Leadless Chip Carrier Solder Joints during Power Cycling," *IEEE Trans. Comp., Hybrids Mfg. Tech.*, CHMT-**6**(3), pp. 232-236.

[18] Ladani, L.J., and Dasgupta, A., 2008, "Damage Initiation and Propagation in Voided Pb-free Solder Joints: Modeling and Experiment," *ASME J. Electronic Packaging*, **130**(1), pp. 011008-1-11.

[19] Qu, J., and Wong, C. P., 2002, "Effective Elastic Modulus of Underfill Material for Flip-chip Applications," *IEEE Trans. Components and Packaging Tech.*, **25**(1), pp. 55.

[20] Khan, A.S., and Wang, X., 2001, *Strain Measurements and Stress Analysis,* Prentice Hall, New Jersey.

[21] Regtien, P. P. L., 2004, *Measurement Science for Engineers,* Kogan Page Science, London, UK.

[22] Neubert, H. K. P., 1968, *Strain Gauges: kinds and uses,* The Chaucer Press, London, UK.

[23] Uttam, D., Culshaw, B., Ward, J. D., and Carter, D., 1985, "Interferometric Optical Fibre Strain Measurement," *J. Physics E*, Scientific Instruments, **18**, pp. 290-293.

[24] Chu, L., Que, L., and Gianchandani, Y., "Measurements of Material Properties Using Differential Capacitive Strain Sensors", *J. Microelectromechanical Systems*, Madison, Wisconsin, **11**(5), pp. 489-497.

[25] Amor, A. B., Budde, T., and Gatzen, H.H., 2004, "A Magnetoelastic Microtransformer-based Microstrain Gauge," *Sensors and Actuators A*, Physical, **129**(1-2), pp. 41-44.

[26] Williams, S. R., 1922, "The Magnetic-mechanical Analysis of Ferromagnetic Substances, its Bearing on Theories of Magnetization," Oberlin, Ohio, **22**(9), pp. 859-871.

[27] Bydzovsky, J., Kraus, L.L., Svec, P., and Pasquale, M, 2004, "Magnetoelastic Strain Sensors for the Outdoors Application." *J. Magnetism and Magnetic Materials*, Proceedings of the International Conference on Magnetism (ICM 2003), **272-276**(1), pp. 1743-1745.

[28] Ladani., L.J., "Mechanical Properties Testing Device and Method," utility patent filed, 61/073,080, May 2009.

[29] Ladani, L.J., and Rodriguez, O., 2010, "Dual Piezo-Actuator-Force Sensor MEMS Device for Strain Measurements," under review.

[30] Jaffe, H., and Berlincourt, D.A., 1965, "Piezoelectric Transducer Materials," Proceedings of the IEEE, Cleveland, Ohio, **55**(10), pp. 1372-1386.

[31] Ikeda, T., 1996, *Fundamentals of Piezoelectricity,* Oxford Science Publications, Oxford, UK, pp. 16-32, 225.

[32] Chu, T. D., 1992, "High Frequency Breakdown Voltage", Superconducting Super Collider Laboratory, Dallas, Texas, pp. 1.

[33] Kim, S. G., 2004, "Piezoelectricity," PFD presentation, Massachusetts Institute of Technology, http://ocw.mit.edu/courses/mechanical-engineering/2-76-multi-scale-system-design-fall-2004/lecture-notes/lecture_7prt2.pdf, slide 17.

APPENDICES

APPENDIX A

ANSYS CODE FOR GENERATING 3D IC SOLID MODEL: PRE-PROCESSING

```
/config,nres,1000000
/PREP 7

!wpro,-90.000000,,

ET, 1, SOLID185,,0,0,,,0,0
KEYOPT, 1, 10, 0

!material number 1--SOLDER BALL
MP,REFT,1,298
MP,ALPX,1,1.16e-5                   !iso-thermal expansion

MPTEMP,1,198,248,298,348,398            !linear isotropic
MPDATA,EX,1,1,20333e-6,19219e-6,18135e-6,16932e-6,15907e-6
MPDATA,NUXY,1,1,0.3,0.3,0.3,0.3,0.3


TB,MISO,1,5,14
TBTEMP,198,1            !temperature 1

TBMODIF,1,1,0.001
TBMODIF,1,2,20.33e-6
TBMODIF,2,1,0.004
TBMODIF,2,2,25.239e-6
TBMODIF,3,1,0.006
TBMODIF,3,2,28.775e-6
TBMODIF,4,1,0.008
TBMODIF,4,2,31.581e-6
TBMODIF,5,1,0.01
TBMODIF,5,2,40.833e-6
TBMODIF,6,1,0.02
TBMODIF,6,2,42.474e-6
TBMODIF,7,1,0.03
TBMODIF,7,2,48.425e-6
TBMODIF,8,1,0.04
TBMODIF,8,2,53.146e-6
TBMODIF,9,1,0.05
TBMODIF,9,2,57.123e-6
TBMODIF,10,1,0.06
TBMODIF,10,2,60.539e-6
TBMODIF,11,1,0.07
TBMODIF,11,2,63.69e-6
TBMODIF,12,1,0.08
TBMODIF,12,2,66.5e-6
TBMODIF,13,1,0.09
TBMODIF,13,2,60.882e-6
TBMODIF,14,1,0.1
TBMODIF,14,2,71.477e-6

TBTEMP,248,2      !temperature 2
TBMODIF,1,1,0.001
TBMODIF,1,2,19.219e-6
TBMODIF,2,1,0.004
TBMODIF,2,2,24.984e-6
TBMODIF,3,1,0.006
TBMODIF,3,2,28.22e-6
TBMODIF,4,1,0.008
TBMODIF,4,2,30.767e-6
```

```
TBMODIF,5,1,0.01
TBMODIF,5,2,32.9e-6
TBMODIF,6,1,0.02
TBMODIF,6,2,40.516e-6
TBMODIF,7,1,0.03
TBMODIF,7,2,45.764e-6
TBMODIF,8,1,0.04
TBMODIF,8,2,49.895e-6
TBMODIF,9,1,0.05
TBMODIF,9,2,53.357e-6
TBMODIF,10,1,0.06
TBMODIF,10,2,56.358e-6
TBMODIF,11,1,0.07
TBMODIF,11,2,59.029e-6
TBMODIF,12,1,0.08
TBMODIF,12,2,61.445e-6
TBMODIF,13,1,0.09
TBMODIF,13,2,63.658e-6
TBMODIF,14,1,0.1
TBMODIF,14,2,65.705e-6


TBTEMP,298,3        !temperature 3
TBMODIF,1,1,0.001
TBMODIF,1,2,18.135e-6
TBMODIF,2,1,0.004
TBMODIF,2,2,24.195e-6
TBMODIF,3,1,0.006
TBMODIF,3,2,27.075e-6
TBMODIF,4,1,0.008
TBMODIF,4,2,29.324e-6
TBMODIF,5,1,0.01
TBMODIF,5,2,31.197e-6
TBMODIF,6,1,0.02
TBMODIF,6,2,37.811e-6
TBMODIF,7,1,0.03
TBMODIF,7,2,42.312e-6
TBMODIF,8,1,0.04
TBMODIF,8,2,45.827e-6
TBMODIF,9,1,0.05
TBMODIF,9,2,48.735e-6
TBMODIF,10,1,0.06
TBMODIF,10,2,51.282e-6
TBMODIF,11,1,0.07
TBMODIF,11,2,53.523e-6
TBMODIF,12,1,0.08
TBMODIF,12,2,55.524e-6
TBMODIF,13,1,0.09
TBMODIF,13,2,57.387e-6
TBMODIF,14,1,0.1
TBMODIF,14,2,59.089e-6


TBTEMP,348,4        !temperature 4

TBMODIF,1,1,0.001
TBMODIF,1,2,16.932e-6
TBMODIF,2,1,0.004
TBMODIF,2,2,22.736e-6
TBMODIF,3,1,0.006
TBMODIF,3,2,25.207e-6
TBMODIF,4,1,0.008
TBMODIF,4,2,27.121e-6
```

```
TBMODIF,5,1,0.01
TBMODIF,5,2,28.705e-6
TBMODIF,6,1,0.02
TBMODIF,6,2,34.24e-6
TBMODIF,7,1,0.03
TBMODIF,7,2,37.96e-6
TBMODIF,8,1,0.04
TBMODIF,8,2,40.834e-6
TBMODIF,9,1,0.05
TBMODIF,9,2,43.228e-6
TBMODIF,10,1,0.06
TBMODIF,10,2,45.281e-6
TBMODIF,11,1,0.07
TBMODIF,11,2,47.09e-6
TBMODIF,12,1,0.08
TBMODIF,12,2,48.719e-6
TBMODIF,13,1,0.09
TBMODIF,13,2,50.207e-6
TBMODIF,14,1,0.1
TBMODIF,14,2,51.565e-6
TBTEMP,398,5       !temperature 5

TBMODIF,1,1,0.001
TBMODIF,1,2,15.907e-6
TBMODIF,2,1,0.004
TBMODIF,2,2,20.435e-6
TBMODIF,3,1,0.006
TBMODIF,3,2,22.446e-6
TBMODIF,4,1,0.008
TBMODIF,4,2,23.991e-6
TBMODIF,5,1,0.01
TBMODIF,5,2,25.263e-6
TBMODIF,6,1,0.02
TBMODIF,6,2,29.658e-6
TBMODIF,7,1,0.03
TBMODIF,7,2,32.575e-6
TBMODIF,8,1,0.04
TBMODIF,8,2,34.818e-6
TBMODIF,9,1,0.05
TBMODIF,9,2,36.663e-6
TBMODIF,10,1,0.06
TBMODIF,10,2,38.242e-6
TBMODIF,11,1,0.07
TBMODIF,11,2,39.631e-6
TBMODIF,12,1,0.08
TBMODIF,12,2,40.875e-6
TBMODIF,13,1,0.09
TBMODIF,13,2,42.004e-6
TBMODIF,14,1,0.1
TBMODIF,14,2,43.041e-6
!define the implicit creep properties for the solder material

TB,CREEP,1,1,4,8
TBTEMP,298
TBDATA,1,882.35,0.111e6,4,8580

!material number 2--Die
MP,REFT,2,298
MP,ALPX,2,2.33e-6
Mp,EX,2,191E-3
MP,NUXY,2,0.3
```

```
*ask, underfill_E, Enter Modulus of elasticity for Underfill material
in GPa, 3
underfill_E=underfill_E/1000
!MATERIAL NUMBER 3--Underfill
MP,REFT,3,298
MP,ALPX,3,30E-6
MP,EX,3,underfill_E
MP,NUXY,3,0.3

!MATERIAL NUMBER 4-- TB SUBSTRATE
MP,REFT,4,298
MP,ALPX,4,15E-6
MP,EX,4,26E-3
MP,NUXY,4,0.39

!MATERIAL NUMBER 5--MOLDING COMPOUND
MP,REFT,5,298
MP,ALPX,5,9E-6
MP,EX,5,15.792E-3
MP,NUXY,5,0.3

! MATERIAL NUMBER 6 - TSV via
MP, REFT, 6, 298
MP, ALPX, 6, 1.43e-5
MP, EX, 6, 0.171
MP, PRXY, 6, 0.35
TB, BISO, 6,1 !bilinear isotropic
TBTEMP,298
TBDATA, 1, 0.0001728, 0.0005171 !c1=yld stss, c2=tang mod

*ask, tuf, Enter thickness of the underfill in microns:, 20
*ask, Dtsv, Enter diameter of the TSV in microns:, 10
!*ask, ptsv, Enter TSV pitch in microns:, 45
*ask, ptsv, Enter TSV pitch in microns:, 70

f = 5 !width of tsv
th= 10 !thickness of material
NUMSTR,VOLUME,1
BLC4, 0, 0, 5*Dtsv, (ptsv/2)-(3*Dtsv)/4,th
BLC4, 0, (ptsv/2)-(3*Dtsv)/4,5*Dtsv, Dtsv/4, th
BLC4, 0, (ptsv/2)-(Dtsv/2),5*Dtsv, Dtsv, th
BLC4, 0, (ptsv/2)+(Dtsv/2), 5*Dtsv, Dtsv/4, th
BLC4, 0, (ptsv/2)+(3*Dtsv)/4,5*Dtsv, (ptsv/2)-(3*Dtsv)/4,th
BLC4,5*Dtsv,0,tuf,ptsv,th

R= sqrt ((tuf/2)*(tuf/2) + (3*Dtsv/4)*(3*Dtsv/4))
NUMSTR,VOLUME,7
CYL4, 5*Dtsv+(tuf/2),  Ptsv/2, R, ,, ,th

ASEL, s, area, , 35,36,1
VSBA,7, all
VDELE, 8,9,1
VPLOT

NUMSTR, VOLUME, 10
BLC4, 5*Dtsv, (Ptsv/2)-(3*Dtsv/4), f, Dtsv/4,th
BLC4, 5*Dtsv, (Ptsv/2)+(Dtsv/2), f, Dtsv/4,th

BLC4, 5*Dtsv+tuf, (ptsv/2)-(3*Dtsv/4), -f, Dtsv/4,th
BLC4, 5*Dtsv+tuf, (ptsv/2)+(3*Dtsv/4), -f, -Dtsv/4,th
BLC4, 5*Dtsv, (ptsv/2)-(Dtsv/2), f, Dtsv,th
BLC4, 5*Dtsv+tuf, (ptsv/2)-(Dtsv/2), -f, Dtsv,th
BLC4, 5*Dtsv+f, (ptsv/2)-(Dtsv/2), tuf-(2*f), Dtsv,th
```

```
VSEL, s, volume, , 1,2,1 !attribute to die
VSEL, a, volume, , 4,5,1
VATT, 2,,1,0,all

VSEL, s, volume, , 3,3,0 !attribute to TSV
VSEL, a, volume, , 11,16,1
VATT, 6,,1,0,all

ALLSEL, all
ASEL, s, area, , 53,54,1
VSBA, 6, all

ASEL, s, area, , 39,56,17
ASEL, a, area, , 60,62,2
ASEL, a, area, , 65,67,2
ASEL, a, area, , 72,73,1
ASEL, a, area, , 89,90,1
VSBA, 10, all
VPLOT
VDELE, 22,22,1
VSEL, s, volume, , 18,19,1 !attribute to underfill
VATT, 3,,1,0,all
VSEL, s, volume, , 20,21,1 !attribute to solder ball
VSEL, a, volume, , 17, 17,0
VATT, 1,,1,0,all
NUMMRG, all

LSEL, s, line, ,5,7,2
LSEL, a, line, ,19,19,0
!LSEL, a, line, ,30,32,1
LSEL, a, line, ,43,43,0
!LSEL, a, line, ,54,56,1
!LSEL, a, line, ,186,188,2
!LSEL, a, line, ,152,152,0
!LSEL, a, line, ,164,166,2
LESIZE,all, , ,3, , , , ,0

LSEL, s, line, ,30,32,2
LSEL, a, line, ,152,152,0
LSEL, a, line, ,164,166,2

LSEL, a, line, ,6,8,2
LSEL, a, line, ,54,56,2
LSEL, a, line, ,186,188,2

LESIZE,all, , ,2, , , , ,0

LSEL, s, line, ,65,67,2
LSEL, a, line, , 62,64,2
LESIZE,all, , ,10, , , , ,0

!To change the solder ball mesh
LSEL, s, line, ,175,177,2!!!
LESIZE,all, , ,5, , , , ,0
LSEL, s, line, , 99, 106, 1
LESIZE,all, , ,5, , , , , 0


LSEL, s, line, ,18,20,2
LSEL, a, line, ,42,44,2
LSEL, a, line, ,77,79,1
LSEL, a, line, ,115,116,1
LSEL, a, line, ,63,68,5
LSEL, a, line, ,127,129,1
```

```
LSEL, a, line, ,130,140,10
LSEL, a, line, ,139,142,3
LESIZE,all, , ,1, , , , , 0

LSEL, s, line, , 70,70,0
LESIZE,all, , ,2, , , , , 0

ASEL, all
ADELE, 41,44,1
ADELE, 46,49,1
LSEL, all
LDELE, 81,84,1
LDELE, 86,87,1
LDELE, 91,92,1
LDELE, 94,95,1

ALLSEL, all
ADELE, all

VGEN, 2,all, , ,5*Dtsv+tuf, , , 0,0,0
VGEN, 2,all, , ,2*(5*Dtsv+tuf), , , 0,0,0

VCLEAR,3
VSEL, s, volume, , 3,3,0 !change to die
VATT, 2,,1,0,all

NUMSTR, volume, 100
BLC4, 0,0,-190,(ptsv/2)-(3*Dtsv/4),th
BLC4, 0,(ptsv/2)-(3*Dtsv/4), -190, Dtsv/4,th
BLC4, 0, (ptsv/2)-(Dtsv/2), -190, Dtsv,th
BLC4, 0, (ptsv/2)+(Dtsv/2), -190, Dtsv/4,th
BLC4, 0,(ptsv/2)+(3*Dtsv/4), -190, (ptsv/2)-(3*Dtsv/4),th

BLC4, 4*(5*Dtsv+tuf),0, 250,(ptsv/2)-(3*Dtsv/4),th
BLC4, 4*(5*Dtsv+tuf),(ptsv/2)-(3*Dtsv/4), 250, Dtsv/4,th
BLC4, 4*(5*Dtsv+tuf), (ptsv/2)-(Dtsv/2), 250, Dtsv,th
BLC4, 4*(5*Dtsv+tuf), (ptsv/2)+(Dtsv/2), 250, Dtsv/4,th
BLC4, 4*(5*Dtsv+tuf),(ptsv/2)+(3*Dtsv/4), 250, (ptsv/2)-(3*Dtsv/4),th

NUMMRG, all

VSEL, s, volume, , 100,104,1 !attribute to Molding compound
VATT, 5,,1,0,all
VSEL, s, volume, , 105,109,1 !attribute to substrate
VATT, 4,,1,0,all

LSEL, s, line, ,457,459,2
LSEL, a, line, ,471,483,12
LSEL, a, line, ,495,507,12
LESIZE,all, , ,10, , , , , 0!!

!LSEL, s, line, ,460,484,24
!LSEL, s, line, ,460,460,0
!LSEL, a, line, ,508,508,0
!LESIZE,all, , ,3, , , , , 0

LSEL, s, line, ,484,484,0
!LSEL, a, line, ,542,542,0

LSEL, a, line, ,460,508,48
!LSEL, a, line, ,518,566,48

LESIZE,all, , ,2, , , , , 0
```

```
LSEL, s, line, ,472,496,24
LESIZE,all, , ,1, , , , , 0

LSEL, s, line, ,517,519,2
LSEL, a, line, ,531,543,12
LSEL, a, line, ,555,567,12
LESIZE,all, , ,5, , , , , 0

LSEL, s, line, ,518,542,24
LSEL, a, line, ,566,566,0
LESIZE,all, , ,2, , , , , 0

LSEL, s, line, ,530,554,24
LESIZE,all, , ,1, , , , , 0

LSEL, s, line, ,512,571,59
LESIZE,all, , ,2, , , , , 0

VSEL, all
VSWEEP, all

inc=5000/ptsv
realinc=NINT(inc)
dif = realinc-inc

*IF, dif, GT, 0.,THEN
realinc = realinc - 1
*ENDIF

! Copying everything up
*DO, i, 1,realinc-1,1
VSEL, s, volume, , 1,5,1
VSEL, a, volume, , 10,68,1
VSEL, a, volume, , 100,109,1
VGEN, 2,all, , , ,ptsv*i , , 0,0,0
*ENDDO
NUMMRG, all
VSEL, all
extra = 5000-realinc*ptsv

NUMSTR, line, 60000

NUMSTR, volume, 10000
BLC4, 0, ptsv*inc, -190, 1000,th
BLC4, 0, ptsv*inc, 5*Dtsv, 1000,th
BLC4, 5*Dtsv, ptsv*inc, tuf, 1000,th
BLC4, 5*Dtsv+tuf, ptsv*inc, 5*Dtsv, 1000,th
BLC4, 10*Dtsv+tuf, ptsv*inc, tuf,1000,th
BLC4, 2*(5*Dtsv+tuf), ptsv*inc, 5*Dtsv, 1000,th
BLC4, 2*(5*Dtsv+tuf)+5*Dtsv, ptsv*inc, tuf,1000,th
BLC4, 3*(5*Dtsv+tuf), ptsv*inc, 5*Dtsv, 1000,th
BLC4, 3*(5*Dtsv+tuf)+5*Dtsv, ptsv*inc, tuf, 1000,th
BLC4, 4*(5*Dtsv+tuf), ptsv*inc, 250, 1000,th

VSEL, s, volume, , 10000, 10008,1
VATT, 5, , 1, 0, all
VSEL, s, volume, , 10009, 10009, 0
VATT, 4, , 1, 0, all

NUMMRG, all

LSEL, s, line, ,60004, 60006,2
LSEL, a, line, ,60028, 60030,2
LSEL, a, line, ,60052,60054,2
```

```
LSEL, a, line, ,60076,60078,2
LSEL, a, line, ,60100,60102,2
LESIZE, all, , ,10, , , , ,0!!

LSEL, s, line, ,60112,60114,2
LESIZE, all, , ,5, , , , ,0

LSEL, s, line, ,60016,60018,2
LSEL, a, line, ,60040,60042,2
LSEL, a, line, ,60064,60066,2
LSEL, a, line, ,60088,60090,2
LESIZE, all, , ,3, , , , ,0

LSEL, s, line, ,60005,60007,2
LSEL, a, line, ,60017,60029,12
LSEL, a, line, ,60041,60053,12
LSEL, a, line, ,60065,60077,12
LSEL, a, line, ,60089,60101,12
LSEL, a, line, ,60113,60113,0
LESIZE, all, , ,15, , , , ,0

LSEL, s, line, ,60008,60118,110
LESIZE, all, , ,2, , , , ,0

VSEL, s, volume, ,10000,10009,1
VSWEEP, all

*IF, dif, NE, 0, THEN
NUMSTR, line, 61000
NUMSTR, volume, 10100
BLC4, 0, ptsv*realinc, -190, extra,th
BLC4, 0, ptsv*realinc, 5*Dtsv, extra,th
BLC4, 5*Dtsv, ptsv*realinc, tuf, extra,th
BLC4, 5*Dtsv+tuf, ptsv*realinc, 5*Dtsv, extra,th
BLC4, 10*Dtsv+tuf, ptsv*realinc, tuf,extra,th
BLC4, 2*(5*Dtsv+tuf), ptsv*realinc, 5*Dtsv, extra,th
BLC4, 2*(5*Dtsv+tuf)+5*Dtsv, ptsv*realinc, tuf,extra,th
BLC4, 3*(5*Dtsv+tuf), ptsv*realinc, 5*Dtsv, extra,th
BLC4, 3*(5*Dtsv+tuf)+5*Dtsv, ptsv*realinc, tuf, extra,th
BLC4, 4*(5*Dtsv+tuf), ptsv*realinc, 250, extra,th

VSEL, s, volume, , 10100,10100,0
VATT, 5,,1,0,all
VSEL, s, volume, , 10101,10101,0
VATT, 2,,1,0,all
VSEL, s, volume, , 10102,10102,0
VATT, 3,,1,0,all
VSEL, s, volume, , 10103,10103,0
VATT, 2,,1,0,all
VSEL, s, volume, , 10104,10104,0
VATT, 3,,1,0,all
VSEL, s, volume, , 10105,10105,0
VATT, 2,,1,0,all
VSEL, s, volume, , 10106,10106,0
VATT, 3,,1,0,all
VSEL, s, volume, , 10107,10107,0
VATT, 2,,1,0,all
VSEL, s, volume, , 10108,10108,0
VATT, 3,,1,0,all
VSEL, s, volume, , 10109,10109,0
VATT, 4,,1,0,all

NUMMRG, all
LSEL, s, line, ,61005,61007,2
```

```
LSEL, a, line, ,61017,61029,12
LSEL, a, line, ,61041,61053,12
LSEL, a, line, ,61065,61077,12
LSEL, a, line, ,61089,61101,12
LSEL, a, line, ,61113,61113,0
LESIZE, all, , ,1, , , , ,0

VSEL, s, volume, ,10100,10109,1
VSWEEP, all

*ENDIF

NUMMRG, all
VPLOT
/NUMBER, 1
/PNUM,MAT,1

!!!!!!!!! Applying constraints in areas

ASEL,S,LOC,Z,0
DA, all, UZ, 0

ASEL,S,LOC,Y,0
DA, all, UY, 0

KSEL, s, kp, , 272,272,0
DK, all, all

nummrg, all



allsel,all
tref,298
toffst,0
```

APPENDIX B

ANSYS CODE FOR GENERATING 3D IC SOLID MODEL: SOLUTION

```
/solu
outres,erase
antype,static,new          !specifies new static analysis
solcontrol,on              !turn on the optimized nonlinear solver
nlgeom,on                  !turn on the large deformation effect
lnsrch,auto                !Auto line search
autots,on                  !automated time stepping
rate,1                     !Turn on creep
crplim,0.25                !creep criterion
!cutcontrol,crplimit,0.25,1  !specifies cutcontrol of creep
bfunif,temp,298            !specifies initial condition
lswrite,init               !reset load step file number
!*************************************************************************
**
! step 1-16                   !temperature up 6 degree in one minute
*do,i,1,16                 !for i=1 to 16
ptime1=60*i                !define time parameter1
ptemp=298+i*6              !define temp parameter
time,ptime1                !time at the end of step 1
nsubst,,100                !specifies the maximum number of substeps
deltim,3,5e-16,15,on     !time increment
kbc,0                     !ramped load
bfunif,temp,ptemp          !apply temperature load
outres,all                      !specifies the results file
lswrite                    !write the load step file fcoc50-1.S1
*enddo
!*************************************************************************
***

! step 17                    !temperature up 4 degree in one minute
time,1000
ptime1=1000                  !time at the end of step 1
nsubst,,100                !specifies the maximum number of substeps
deltim,3,5e-16,10,on     !time increment
kbc,0                      !ramped load
bfunif,temp,398            !apply temperature load
outres,all
lswrite                    !write the load step file fcoc50-1.S3
!*************************************************************************
***

!step 18                    !temperature dwell for 300 seconds
time,1300
ptime1=1300                  !time at the end of step
nsubst,,100                !specifies the maximum number of substeps
deltim,5,5e-16,20,on    !time increment
kbc,0
bfunif,temp,398                            !stepped load
outres,all
lswrite                    !write the load step file fcoc50-1.S6
!*************************************************************************
****

!step 19                    !temperature dwell for 300 seconds
time,1600
ptime1=1600                  !time at the end of step
nsubst,,100                !specifies the maximum number of substeps
deltim,5,5e-16,20,on    !time increment
```

```
kbc,0                        !stepped load
bfunif,temp,398
outres,all
lswrite                      !write the load step file fcoc50-1.s6
!*************************************************************************
****

!step 20                     !temperature dwell for 300 seconds
time,1900
ptime1=1900                    !time at the end of step
nsubst,,100                  !specifies the maximum number of substeps
deltim,5,5e-16,20,on    !time increment
kbc,0
bfunif,temp,398
outres,all
lswrite                      !write the load step file fcoc50-1.s6
!*************************************************************************
*****
!step 21-56                      !cooling down for 1080 second
*do,i,1,36                   !for i=1 to 36
ptime1=1900+30*i             !define time parameter1
ptemp=398-i*5                !define temp parameter
time,ptime1                  !time at the end of step 1
nsubst,,100                  !specifies the maximum number of substeps
deltim,3,5e-16,15,on     !time increment
kbc,0                          !ramped load
bfunif,temp,ptemp            !apply temperature load
outres,all
lswrite                      !write the load step file fcoc50-1.s7
*enddo
!*************************************************************************
*****

!step 57                      !temperature dwell for 300 seconds
time,3280
ptime1=3280                    !time at the end of step
nsubst,,100                  !specifies the maximum number of substeps
deltim,5,5e-16,20,on    !time increment
kbc,0                        !stepped load
bfunif,temp,218
outres,all
lswrite                      !write the load step file fcoc50-1.s12
!*************************************************************************
****

!step 58                     !temperature dwell for 300 seconds
time,3580
ptime1=3580                    !time at the end of step
nsubst,,100                  !specifies the maximum number of substeps
deltim,5,5e-16,20,on    !time increment
kbc,0                        !stepped load
bfunif,temp,218
outres,all
lswrite                      !write the load step file fcoc50-1.s12
!*************************************************************************
***

! step 59-73                     !temperature going up for 6 degree in
one minute
*do,i,1,15                   !for i=1 to 30
ptime1=3580+60*i             !define time parameter1
ptemp=218+i*6                !define temp parameter
time,ptime1                  !time at the end of step 1
nsubst,,100                  !specifies the maximum number of substeps
```

```
deltim,3,5e-16,10,on     !time increment
kbc,0                      !ramped load
bfunif,temp,ptemp
outres,all
lswrite
*enddo
!*************************************************************************
*****

lssolve,1,73               !solve load steps
finish
```

APPENDIX C

ANSYS CODE FOR GENERATING 3D IC SOLID MODEL: POST-PROCESSING

(SOLDER BALL)

```
/POST1

APPEND,near,,,,0
ETABLE,P1,SEND,PLASTIC
PLETAB,P1,AVG

ETABLE,C1,SEND,CREEP
PLETAB,C1


APPEND,near,,,,4480
ETABLE,P2,SEND,PLASTIC
!PLETAB,P2,AVG

SADD,P3,P2,P1,,-1
!PLETAB,P3,AVG

ETABLE,C2,SEND,CREEP
!PLETAB,C2,AVG
!SADD,P3,P2,P1,,-1
!PLETAB,P3
SADD,C3,C2,C1,,-1
!PLETAB,C3

SADD,P4,P3,C3,,-1
SMULT,PD1,P4,,0.005050
SMULT,CD1,C3,,8.13E-5
SEXP,PD,PD1,,1.25
SEXP,CD,CD1,,0.7143
SADD,TOT,PD,CD
```

APPENDIX D

ANSYS CODE FOR GENERATING 3D IC SOLID MODEL: POST-PROCESSING

(COPPER TSV)

```
/POST1
APPEND,near,,,,0
ETABLE,E1,NL,EPEQ

APPEND,near,,,,4480
ETABLE,E2,NL,EPEQ

SADD,E3,E2,E1,1,-1
SEXP,E4,E3,,-2.4554
SMULT, ETOT, E4,,0.0122
PLETAB,ETOT,NOAV
```

APPENDIX E

ANSYS CODE FOR GENERATING STRAIN MEASURING SYSTEM FOR ELASTIC TEST SPECIMEN: PRE-PROCESSING AND SOLUTION

```
/PREP7
SMRT,OFF
ET, 1, SOLID5, 3 !setting DOF: UX, UY, UZ and VOLT
ET, 2, SOLID185

! Piezoelectric material
MP, DENS, 1, 4.628E-15 ! in microns
MP, PERX, 1, 1.509E-2
MP, PERY, 1, 1.509E-2
MP, PERZ, 1, 1.269E-2
TB, PIEZ, 1, , , 0 ! Setting TBOPT=0 to accept matrices e, c, epsilonS
rather than
                  !d, s, epsilonT

TBDATA, 1, 0,0,-6.623,0,0,-6.623    !Entering e matrix
TBDATA, 7, 0,0,23.24,0,0,0
TBDATA, 13,0,17.03,0, 17.03,0,0

TB, ANEL, 1 !Entering c matrix
TBDATA, 1,1.272e5,8.021e4,8.467e4,0,0,0 !IEEE standard
TBDATA, 7,1.272e5,8.467e4,0,0,0
TBDATA, 12,1.174e5,0,0,0
TBDATA, 16,2.353e4,0,0
TBDATA, 19,2.299e4,0
TBDATA, 21, 2.299e4

!Test specimen (elastic)
!MP,REFT,2,298
!MP,ALPX,2,9E-6
MP,EX,2,15.792E3
MP,NUXY,2,0.3
MP, PERX, 2, 0

! Test specimen (plastic)
!MP, REFT, 6, 298
!MP, ALPX, 6, 1.43e-5
MP, EX, 3, 15.792E3
MP, NUXY, 3, 0.3
TB, BISO, 3,1 !bilinear isotropic
!TBTEMP,298
TBDATA, 1, 91.5, 0.0005171 !c1=yld stss, c2=tang mod
MP, PERX, 3, 0

block,0,5,0,5,0,5
block,0,5,0,5,5,10
block,0,5,0,5,10,15

VSEL, s, volume, , 1,3,2
VATT, 1,,1,0,all
VSEL, s, volume, , 2,2,0
VATT, 2,,2,0,all
NUMMRG, all
ALLSEL, ALL

! Creating line divisions for mesh
```

```
LESIZE,all, , ,10, , , , ,0
VSWEEP, all
ALLSEL, ALL
NUMMRG, all

/SOLU

outres,erase
antype,static,new          !specifies new static analysis
solcontrol,on              !turn on the optimized nonlinear solver
nlgeom,on                  !turn on the large deformation effect
lnsrch,auto                !Auto line search
autots,on                  !automated time stepping

DA, 1, UZ,0
DA, 14,UZ,0
DA, 2, VOLT,0
DA, 8, VOLT,0

*do,i,0,60,10
ptime1=60*i                !define time parameter1
time,ptime1                !time at the end of step 1
nsubst,,100                !specifies the maximum number of substeps
deltim,3,5e-16,15,on     !time increment

DADELE,1,VOLT
DA, 1, VOLT, i

NSEL,ALL
outres,all                      !specifies the results file
lswrite                    !write the load step file fcoc50-1.S1
*enddo

lssolve,1,7               !solve load steps
```

APPENDIX F

ANSYS CODE FOR GENERATING STRAIN MEASURING SYSTEM FOR PLASTIC TEST SPECIMEN: PRE-PROCESSING AND SOLUTION

```
!SOLID5 does not give plastic strain, need to use something else for
test material,
!that supports VOLT DOF

/PREP7
SMRT,OFF
ET, 1, SOLID5, 3 !setting DOF: UX, UY, UZ and VOLT
ET, 2, SOLID185

! Piezoelectric material
MP, DENS, 1, 4.628E-15 ! in microns
MP, PERX, 1, 1.509E-2
MP, PERY, 1, 1.509E-2
MP, PERZ, 1, 1.269E-2
TB, PIEZ, 1, , , 0 ! Setting TBOPT=0 to accept matrices e, c, epsilonS
rather than
                  !d, s, epsilonT

TBDATA, 1, 0,0,-6.623,0,0,-6.623    !Entering e matrix
TBDATA, 7, 0,0,23.24,0,0,0
TBDATA, 13,0,17.03,0, 17.03,0,0

TB, ANEL, 1 !Entering c matrix
TBDATA, 1,1.272e5,8.021e4,8.467e4,0,0,0 !IEEE standard
TBDATA, 7,1.272e5,8.467e4,0,0,0
TBDATA, 12,1.174e5,0,0,0
TBDATA, 16,2.353e4,0,0
TBDATA, 19,2.299e4,0
TBDATA, 21, 2.299e4

!Test specimen (elastic)
!MP,REFT,2,298
!MP,ALPX,2,9E-6
MP,EX,2,15.792E3
MP,NUXY,2,0.3
MP, PERX, 2, 0

! Test specimen (plastic)
!MP, REFT, 6, 298
!MP, ALPX, 6, 1.43e-5
MP, EX, 3, 15.792E3
MP, NUXY, 3, 0.3
TB, BISO, 3,1 !bilinear isotropic
!TBTEMP,298
TBDATA, 1, 91.5, 0.0005171 !c1=yld stss, c2=tang mod
MP, PERX, 3, 0

block,0,5,0,5,0,5
block,0,5,0,5,5,10
block,0,5,0,5,10,15

VSEL, s, volume, , 1,3,2
VATT, 1,,1,0,all
VSEL, s, volume, , 2,2,0
```

```
VATT, 3,,2,0,all
NUMMRG, all
ALLSEL, ALL

! Creating line divisions for mesh

LESIZE,all, , ,10, , , , ,0
VSWEEP, all
ALLSEL, ALL
NUMMRG, all

/SOLU

outres,erase
antype,static,new          !specifies new static analysis
solcontrol,on              !turn on the optimized nonlinear solver
nlgeom,on                  !turn on the large deformation effect
lnsrch,auto                !Auto line search
autots,on                  !automated time stepping

DA, 1, UZ,0
DA, 14,UZ,0
DA, 2, VOLT,0
DA, 8, VOLT,0

*do,i,0,250,25
ptime1=60*i                !define time parameter1
time,ptime1                !time at the end of step 1
nsubst,,100                !specifies the maximum number of substeps
deltim,3,5e-16,15,on     !time increment

DADELE,1,VOLT
DA, 1, VOLT, i

NSEL,ALL
outres,all                      !specifies the results file
lswrite                    !write the load step file fcoc50-1.S1
*enddo


lssolve,1,11               !solve load steps
```